1. Introduction

Epidermal growth-factor receptor (EGFR) is the prototypic member of the EGFR family of receptors, which also contains HER2/neu (ErbB2), HER3 (ErbB3), and HER4 (ErbB4) [1–4]. This family is involved in regulating signaling pathways that are implicated in the proliferation, invasion, migration, survival, adhesion, and differentiation of cancer cells [3,5]. EGFR and/or HER2 are expressed at high levels in many human malignancies of epithelial origin, including lung, breast, head and neck, and bladder cancer [6,7]. They exist as monomeric receptors spanning the plasma membrane and are activated by dimerization after binding to ligands, such as EGF/TGFα, heparin-binding EGF, epiregulin, betacellulin, and amphiregulin. The homodimerization and/or the heterodimerization of EGFR with other family members induces the ligand-specific activation of a number of intracellular signal-transduction cascades, including phospholipase Cγ, phosphatidylinositol-3-kinase (PI3K)-Akt, small G-proteins, Ras. Ras GTPase-activating protein, extracellular signal-regulated kinase (ERK)-1/2, Src family kinases, and signal transducer and activator of transcription (STAT) [8]. So far, no ligand has been identified for HER2, which seems to be the preferred heterodimeric partner for all other members of the EGFR family [9]. In fact, heterodimers containing HER2 have been reported to show greater affinity for ligands [10], to generate more prolonged signals and to enhance the biological effects of EGFR ligands, such as EGF [9,11]. High expression levels of EGFR and/or HER2 are associated with disease progression and poor prognosis in patients with various malignant cancers [4,5,12–14]. EGFR and HER2 proteins are therefore attractive targets for novel anticancer therapies [3,15].

The EGFR tyrosine-kinase inhibitor ZD1839 (Iressa) is a small-molecule anticancer agent and a synthetic anilinoquinazoline [16]. It is orally active and blocks signal-transduction pathways implicated in the proliferation and survival of cancer cells, as well as other host-dependent processes that promote cancer growth [3,17–19]. It shows antiproliferative activity in various different human cancer cell in vitro [20]. ZD1839-induced tumor-growth inhibition in vivo is potentiated by combination with a range of cytotoxic anticancer agents [20–23]. Clinically significant antitumor activity and symptom relief were reported in two phase II trials (known as IDEAL 1 and 2) of ZD1839 monotherapy in patients with advanced non-small-cell lung cancer (NSCLC), all of whom had previously received treatment with platinum-based chemotherapy [24–27]. ZD1839 has now been approved in several countries—including Japan, Australia, and United States—for use in patients with inoperable or recurrent NSCLC.

The humanized anti-HER2 monoclonal antibody trastuzumab (Herceptin) is an anticancer agent that was developed against HER2. Trastuzumab activity is dependent on HER2-expression levels [28–31]. Clinical trials have clearly demonstrated that trastuzumab has significant activity against HER2-positive metastatic breast cancer [32,33].

EGFR and HER2 are overexpressed in 40–80% and 25–30%, respectively, of NSCLC patients [26, 34]. A recent report suggested that they might act in concert to sustain the autonomous proliferation of breast cancer cells [35–38]. Moreover, breast tumors that co-express EGFR and HER2 have a relatively poor prognosis compared with tumors that express only one of these receptors [39–41]. Improved therapeutic effects might therefore be obtained against NSCLC cells expressing both EGFR and HER2 through combined treatment with ZD1839 and trastuzumab.

The present study aimed to determine whether a combination of ZD1839 and trastuzumab showed significant cytotoxicity against NSCLC cells. The effects of this combination treatment are discussed with respect to cell growth, cell signaling and the cell cycle.

2. Materials and methods

2.1. Materials

ZD1839 was provided by AstraZeneca (Macclesfield, UK), trastuzumab was purchased from Chugai Pharmaceutical Company (Tokyo, Japan).

2.2. Cell lines and cell culture

The human NSCLC cell lines A549, NCI-H23, NCI-H727, and NCI-H661, and the human vulval squamous carcinoma cell line A431, were purchased from the American Type Culture Collection (Manassas, VA). Dulbecco's modified Eagle's medium (DMEM) and Roswell Park Memorial Institute (RPMI) 1640 were used as culture media, supplemented with 10% fetal bovine serum (FBS), 100 IU/ml penicillin, and 100 μg/ml streptomycin. A549 and A431 were cultured in DMEM, whilst NCI-H23, NCI-H727, and NCI-H661 were cultured in RPMI 1640. All cells were maintained under standard cell-culture conditions at 37 °C and 5% CO_2 in a humid environment.

2.3. Cell viability assay

For cell viability assays, WST-8 (2-(2-methoxy-4-nitrophenyl)-3-(4-nitophenyl)-5-(2,4-disulfophenyl)-2H-tetrazolium, monosodium salt) assays (Dojindo, Kumamoto, Japan) were used in this study. Briefly, cells were seeded at a density of $3–5 \times 10^3$ cell/well in 96-well plates. After 24 h, various concentrations of ZD1839 and/or trastuzumab were added, as indicated, and the cells were incubated for a further 96 h. Subsequently, the cells were washed with phosphate-buffered salin (PBS) and 10% WST-8 solution for 2 h at 37 °C. Absorbance was measured at 450 nm using a microplate reader model 550 (Bio-Rad Laboratories, Hercules, CA). Absorbance values were expressed as the percentage of untreated controls, and the concentration of ZD1839 and/or trastuzumab resulting in 50% growth inhibition (IC_{50}) was calculated.

2.4. Colony-formation assay

Cells survival were determined by plating 1×10^3 cells in 35-mm dishes. After 24 h, the medium was replaced with medium containing ZD1839 and/or trastuzumab at the concentrations indicated. The cells were incubated in a humidified chamber at 37 °C for 10 days. They were then washed with PBS and fixed with 100% methanol. Finally, the cells were stained with 10% crystal violet in water for at least 2 h at room temperature, and the number of colonies present was counted. Clonogenic survival was expressed as the percentage of colony-forming units present in the treated cultures relative to the untreated controls.

2.5. Cell-cycle analysis

Cells were seeded at a density of 1×10^5 cells/well in six-well plates. After 24 h, the medium was replaced with medium containing ZD 1839 and/or trastuzumab at concentrations of 1 and 1 μM, respectively, as indicated. Cells were incubated in a humidified chamber at 37 °C for 48 h, and then fixed with 70% ethanol, stained with 1 mg/ml propidium iodide (PI), and examined for changes in the cell-cycle distribution using flow cytometry (FACScan: Becton Dickinson).

2.6. Western blot analysis

Cells were cultured in six-well plates until subconfluence, and then incubated with ZD1839 and/or trastuzumab at the indicated concentrations for 3 h at 37 °C. Cells were washed with PBS and lysed in buffer containing 50 mM Tris–HCl, pH 6.8, 10% glycerol, 2% sodium dodecyl sulfate (SDS), and 5% β-mercaptoethanol, and then lysed by sonication. After the removal of cell debris by centrifugation, protein concentrations were determined using the Bio-Rad protein assay (Bio-Rad Laboratories). Cell lysates were boiled for 5 min at 100 °C, and equal amounts of protein (10 μg) were subjected to 7.5–15% SDS-polyacrylamide gel electrophoresis (SDS-PAGE) and transferred to nitrocellulose membranes (Millipore, Bedford, MA). Membranes were blocked with PBS containing 5% milk and 0.1% Tween 20, and then incubated with the following primary antibodies: anti-EGFR (1:2500; BD Transduction Laboratories, Lexington, KY); anti-HER2 (1:50; Zymed Laboratories, San Francisco, CA); anti-HER3 and anti-HER4 (1:500; Neomarkers, Freemont, CA); anti-phospho EGFR (1:2000; Upstate Biotechnology, Lake Placid, NY); anti-phospho HER2, anti-ERK-1/2, anti-phospho ERK-1/2, anti-Akt, anti-phospho Akt, anti-retinoblastoma (Rb), and anti-phospho Rb (1:1000; Cell Signaling Technology, Beverly, MA); and anti-p27, anti-cyclin E and anti-cyclin D1 (1:1000; Santa Cruz Biotechnology, Santa Cruz, CA). After washing three times with Tween 20-PBS (containing 0.1% Tween 20), membranes were

incubated with secondary antibody conjugated to anti-mouse or anti-rabbit horseradish peroxidase (HRP) (Bio-Rad Laboratories). The protein conducts were visualized using the enhanced chemiluminescence Western-blotting detection system (Amersham Pharmacia Biotech). The relative expression was calculated using the NIH Image version 1.62) program (rsb.info.nih.gov/nih-image/download.html).

2.7. Immunoprecipitation and immunoblot analysis

Cells were cultured in 100-mm dishes until subconfluence, and then incubated with ZD1839 at the concentrations indicated for 3 h at 37 °C. Cells were washed with PBS and lysed in NP-40 buffer (50 mM Tris, 1 mM EDTA. 80 mM NaCl, 0.3% NP-40, and 10% glycerol containing 1 mM PMSF,

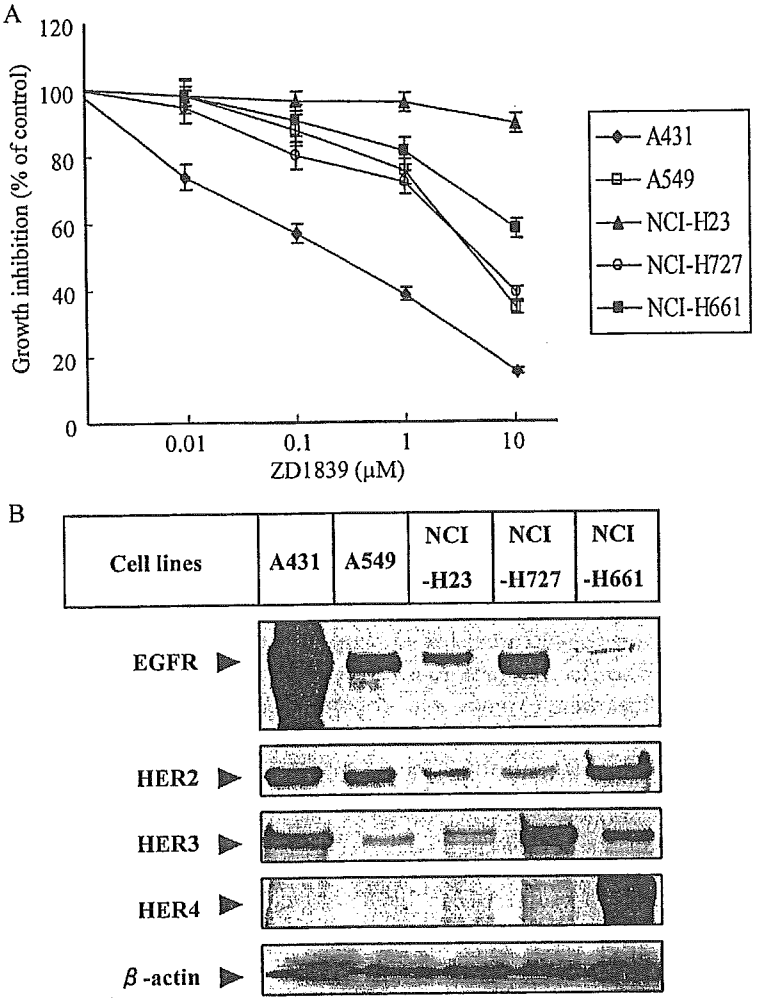

Fig. 1. Effects of ZD1839 on the growth of NSCLC cells and variation in the expression of EGFR family proteins. (A) Cell viability assays were performed as described in Section 2, with various concentrations of ZD1839. Cells ($3–5 \times 10^3$/well) were seeded into 96-well plates. After 24 h, the cells were incubated with ZD1839 for 96 h. The number of viable cells in each well was estimated using WST-8 assays. Each data point represents the mean ± SD of triplicate experiments, expressed as a percentage of the cell growth relative to untreated controls. (B) The expression levels of EGFR family proteins were measured using Western blot analysis. Cells were cultured in six-well plates until subconfluence, and then cells were harvested. Equal amounts of protein were loaded onto a 7.5% SDS-PAGE gel and immunoblotted with the antibodies indicated, as detailed in Section 2. EGFR, HER2, HER3, and HER4 protein levels were determined using anti-EGFR, anti-HER2, anti-HER3, and anti-HER4 antibodies. Similar results were obtained in repeated experiments.

10 μg/ml aprotinin, 10 μg/ml leupeptin, and 1 mM sodium vanadate). For immunoprecipitation, 2 mg of total protein from cell lysates were incubated with appropriate amounts of primary antibody at 4 °C for 3 h. Protein A/G PLUS agarose (15 μl, Santa Cruz Biotechnology) was then added for a further 2 h at 4 °C with rocking. Immnoprecipitates were pelleted by centrifugation and washed three times with lysis buffer. Captured proteins were then eluted by boiling the beads in SDS sample buffer for 5 min at 100 °C. Samples were subjected to 7.5% SDS-PAGE electrophoresis and transferred to nitrocellulose membranes. Immunoblot analysis was performed as described above.

2.8. Statistical analysis

Statistical analysis was performed using the Student's *t*-test. A probability (*P*) level of <0.05 was considered statistically significant.

3. Results

3.1. Differential effects of ZD1839 on NSCLC cell growth and EGFR family protein expression

We first examined the effects of ZD1839 on cell proliferation in four human NSCLC cell lines—A549, NCI-H23, NCI-H727, and NCI-H661—compared with the human vulval squamous carcinoma cell line A431, which is known to be highly susceptible to growth inhibition by ZD1839 [42]. ZD1839 induced dose-dependent growth inhibition in the NSCLC cell lines, and significantly inhibited the proliferation of A431 cells (Fig. 1(A)). Among the NSCLC cell lines, A549 was the most sensitive to ZD1839, whereas NCI-H23 showed the least effects.

The four NSCLC cell lines examined expressed varying amounts of EGFR, HER2, HER3, and HER4 proteins as summarized in Table 1. Consistent with previous findings [42], A431 cells expressed high levels of EGFR (Fig. 1(B)). A549, NCI-H23, and NCI-H727 cells expressed comparable levels of EGFR, whereas little, if any, EGFR was expressed in NCI-H661 cells. Comparable levels of HER2 expression were detected in A549 and NCI-H661 cells, but the levels were much lower in NCI-H23 and NCI-H727 cells. NCI-H727 and NCI-H661cells showed greater levels of HER3 expression than A549 and NCI-H23 cells. By contrast, only NCI-H661 cells expressed high levels of HER4.

3.2. Effects of combination treatment with ZD1839 and trastuzumab on NSCLC cell growth

In the next experiment, we evaluated the effects of various doses of ZD1839 on the growth of NSCLC cells in the presence or absence of trastuzumab at doses of 0.01, 0.1, and 1 μM. A combination of ZD1839 and trastuzumab induced significant growth inhibition in A549 cells (Fig. 2(A)). This combination appeared to have a slight additive effects, or no effects at all, on the growth of NCI-H23, NCI-H727, and NCI-H661 cells (Fig. 2(B), and data not shown). NCI-H23 cells in particular showed no significant growth inhibition.

Table 1
Comparison of protein expression levels of EGFR family and ZD1839-induced growth inhibition

Cell lines	EGFR family protein levels (%)[a]				Growth inhibition[b]
	EGFR	HER2	HER3	HER4	IC_{50} (μM)
A431	270	108	89	<10	0.7
A549	92	69	<10	<10	5.4
NCI-H23	41	15	<10	<10	>10
NCI-H727	100	<10	100	<10	7.6
NCI-H661	<10	100	40	100	>10

[a] Protein expression levels were examined by Western blotting. Further, the indensity of specific staining for each cell lines were quantitatived using a NIH Image, according to the manufacture's instructions. Relative EGFR family levels of five cell lines are presented when normalized by EGFR level in NCI-H727, HER2 level in NCI-H661, HER3 level in NCI-H727, HER4 level in NCI-H661.

[b] ZD1839 concentrations (μM) responsible for 50% growth inhibition in WST-8 assay at 96 h, calculated with data of triplicate experiments.

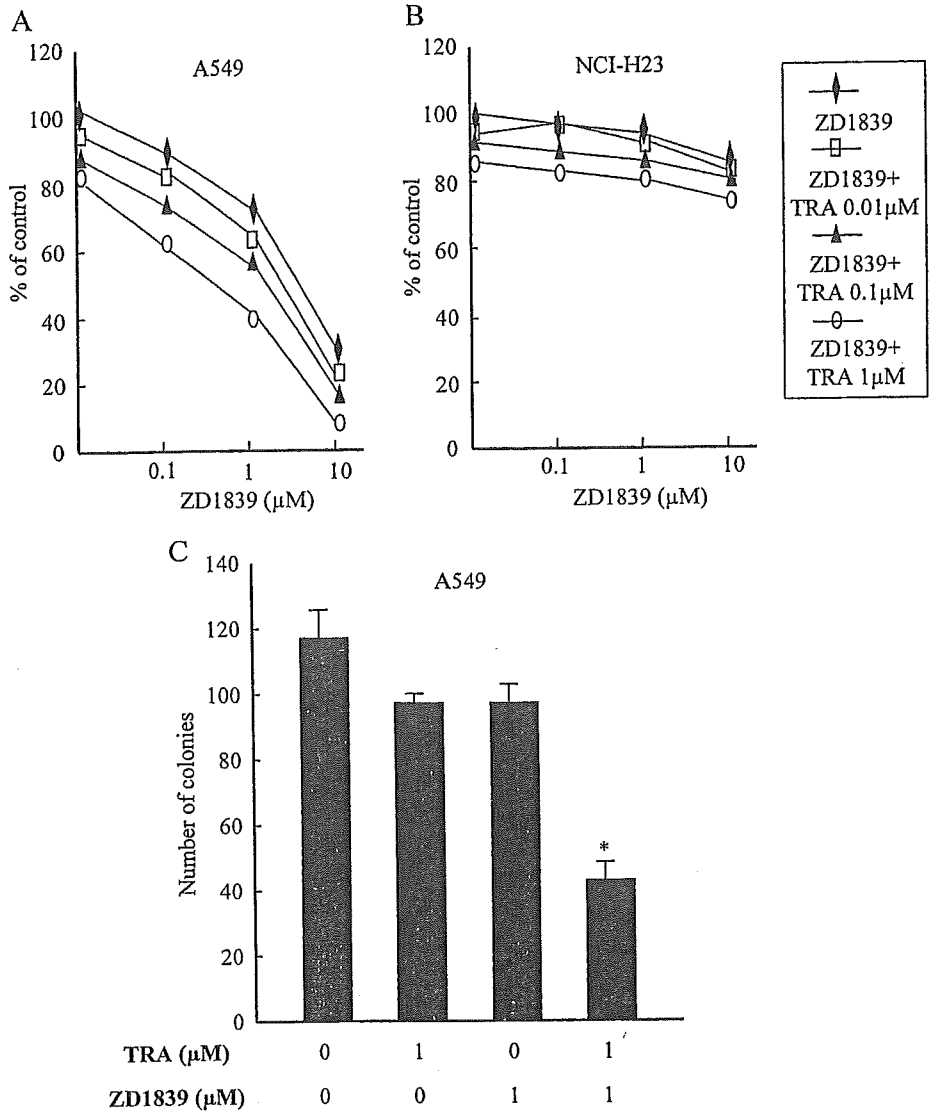

Fig. 2. Effects of combination treatment with ZD1839 and trastuzumab (TRA) on NSCLC cell proliferation and cell-colony survival. (A) A549 cells; (B) NCI-H23 cells. Cells ($3–5\times10^3$/well) were seeded into 96-well plates and incubated the following day with the concentrations of ZD1839 and/or TRA indicated. After 96 h of treatment, the number of viable cells in each well was estimated using WST-8 assays, as described in Section 2. Similar results were obtained in triplicate experiments. The coefficient of variation was always below 10%. For reasons of clarity it is not shown. (C) A549 cells (1×10^3/dish) were seeded in colony-formation assays with the concentrations of ZD1839 and/or TRA indicated, as described in Section 2. Each column represents the mean number of colonies with a diameter >50 μm in three dishes. The bars show the mean $\pm$ SD of triplicate experiments. An asterisk denotes a statistically significant difference ($P<0.05$) compared with the untreated controls or cells treated with either drug alone.

We further evaluated the effects in A549 cells using a colony-formation assay. Combination treatment with ZD1839 at 1 μM and trastuzumab at 1 μM induced significant growth inhibition in A549 cells compared with untreated controls or cells treated with either drug on its own (Fig. 2(C)), These data clearly show that a combination of ZD1839 and trastuzumab produces significant growth inhibition in A549 cells. These effects were not observed in the other cell lines examined (data not shown).

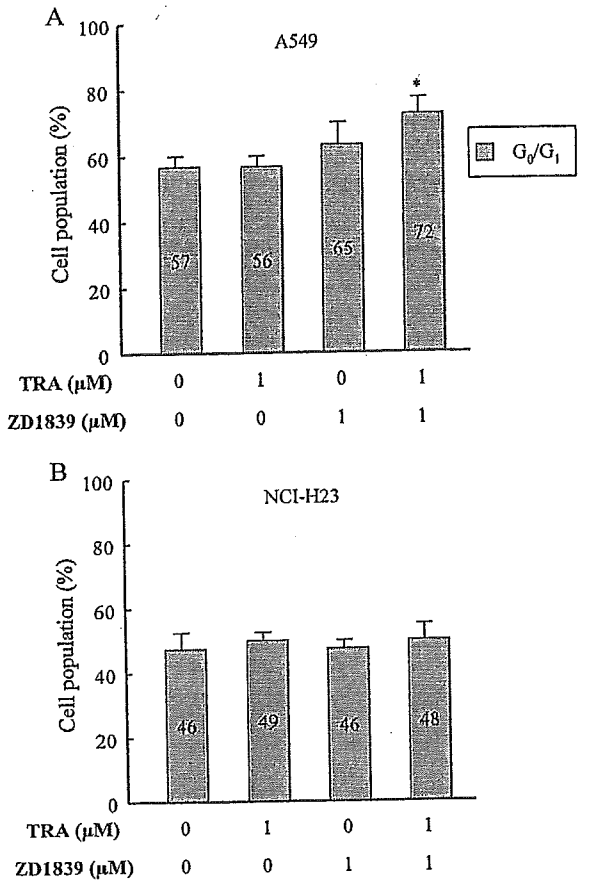

Fig. 3. Effects of combination treatment with ZD1839 and trastuzumab (TRA) on NSCLC cell-cycle progression. (A) A549 cells; (B) NCI-H23 cells. Cells were treated with ZD1839 at 1 μM and/or TRA at 1μM for 48 h. They were then fixed with 70% ethanol, stained with PI, and changes in the cell-cycle distribution were examined using flow-cytometric analysis, as described in Section 2. The numbers of cells percentage in the G_0/G_1 phase are shown in the bar graph. The data represent the mean values and the bars indicated the SD of triplicate experiments. An asterisk denotes a statistically significant difference ($P<0.05$) compared with the untreated controls or cells treated with either drug alone. Similar results were obtained in repeated experiments.

3.3. Effects of combination treatment with ZD1839 and trastuzumab on cell-cycle progression and expression of cell-cycle-related proteins

We then examined the cell growth inhibitory effects of a combination of ZD1839 and trastuzumab on cell-cycle progression using FACScan. In A549 cells, a combination of ZD1839 at 1 μM and trastuzumab at 1 μM produced a significant increase in the numbers of cells in the G_0/G_1 phase compared with untreated control cells or those treated with either drug on its own (Fig. 3(A)). This was accompanied by a corresponding decrease in the number of A549 cells in the S and G_2/M phases. Combination treatment therefore induced G_1 arrest in A549 cells. By contrast, no significant changes were observed in cell-cycle distribution in NCI-H23, NCI-H727, and NCI-H661 cells after combination treatment (Fig. 3(B), and data not shown). We next examined the expression of cell-cycle regulators, such as p27 and cyclin E or D1, which are essential for G_1/S phase progression, in NSCLC cells. Combination treatment increased the expression of cyclin-dependent kinase inhibitor p27, but decreased the expression of cyclin E or D1 (Fig. 4). The phosphorylation of Rb (Ser-780) protein was also inhibited compared with the untreated controls or cells treated with either drug alone. By contrast, the combination treatment had no significant effects on the expression of p27, cyclin E or D1, and Rb phosphorylation in NCI-H23 cells.

3.4. EGFR and HER2-induced cell-growth signaling in NSCLC cells after combination treatment with ZD1839 and trastuzumab

HER2 as well as EGFR activates a number of cytoplasmic signal transduction pathways such as the PI3K-Akt and Ras-MAP kinase. We then evaluated the effects of combination of ZD1839 and trastuzumab on EGFR, HER2, ERK-1/2, and Akt (ser-473) phosphorylation in A549 and NCI-H23 cells under basal growth conditions in the presence of 10% serum. Combination treatment with ZD1839 at 1 μM and trastuzumab at 1 μM produced significant inhibition of phosphorylation of EGFR and HER2 in A549 cells, compared with treatment with either drug alone (Fig. 5). Moreover, the combination treatment also significantly inhibited the phosphorylation of ERK-1/2 and Akt in A549 cells. No effects were detected in NCI-H23 cells.

3.5. Formation of constitutive EGFR/HER2 heterodimers in NSCLC cells

A combination of ZD1839 and trastuzumab was found to block EGFR and HER2 signaling in A549

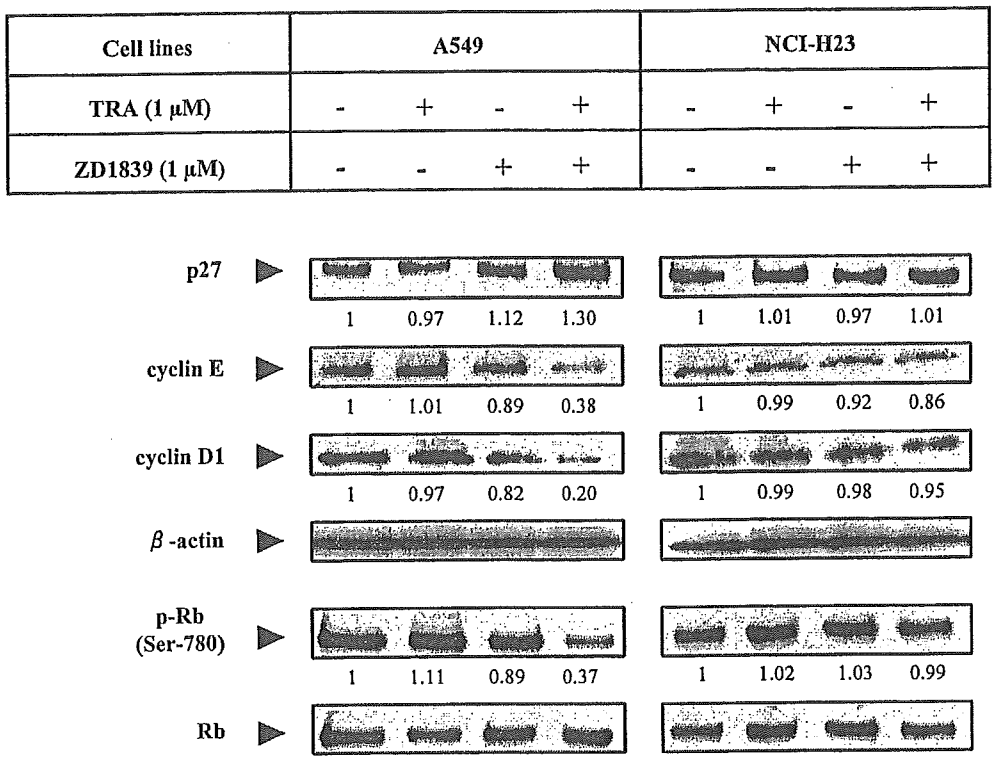

Fig. 4. Effects of combination treatment with ZD1839 and trastuzumab (TRA) on the expression of cell-cycle related proteins. The expression levels of p27, cyclin E or D1, and Rb were measured in drug-sensitive A549 and drug-resistant NCI-H23) cells. Cells were treated for 48 h with ZD1839 at 1 μM and/or TRA at 1 μM. Equal amounts of protein were separated by SDS-PAGE and subjected to immunoblot analysis with the antibodies indicated, as detailed in Section 2. p27 and cyclin E or D1 levels were determined using anti-p27 and anti-cyclin E or D1 antibodies, respectively. Rb activity was determined using an anti-phospho Rb antibody, and Rb protein levels were evaluated using anti-Rb antibody. Similar results were obtained in repeated experiments. Values indicate the density of the bands.

cells but not in NCI-H23 cells. The EGFR/HER2 heterodimer is frequently detected in cancer cell lines in culture [43,44] and is thought to have an important role in cell signaling. We therefore compared the formation of EGFR/HER2 heterodimers in A549 and NCI-H23 cells. Immunoprecipitation and immunoblot analysis revealed the formation of constitutive EGFR/HER2 heterodimers in A549 cells (Fig. 6), which showed a twofold increase in the presence of ZD1839. By contrast, NCI-H23) cells showed little, if any, formation of constitutive EGFR/HER2 heterodimers.

4. Discussion

EGFR and HER2 are important molecular targets for anticancer drugs. ZD1839 (Iressa), which selectively inhibits EGFR tyrosine kinase, is effective in patients with advanced NSCLC. The humanized anti-HER2 antibody trastuzumab (Herceptin) is effective against metastatic breast cancer [32,33]. Ye et al. [45] reported that a combination of trastuzumab and the anti-EGFR monoclonal antibody C225 had an additive antiproliferative effect in ovarian cancer cells. Moreover, several studies have demonstrated synergistic growth inhibition by trastuzumab and ZD1839 in breast cancer cells [35–38]. In the present study, we evaluated the potential cooperative antiproliferative effects of ZD1839 and trastuzumab on NSCLC cells in culture. These drugs showed significant cytotoxic effects on the proliferation of ZD1839-sensitive NSCLC cells in both WST-8 and colony-formation assays. By contrast, the combination treatment had either a slight additive effects or

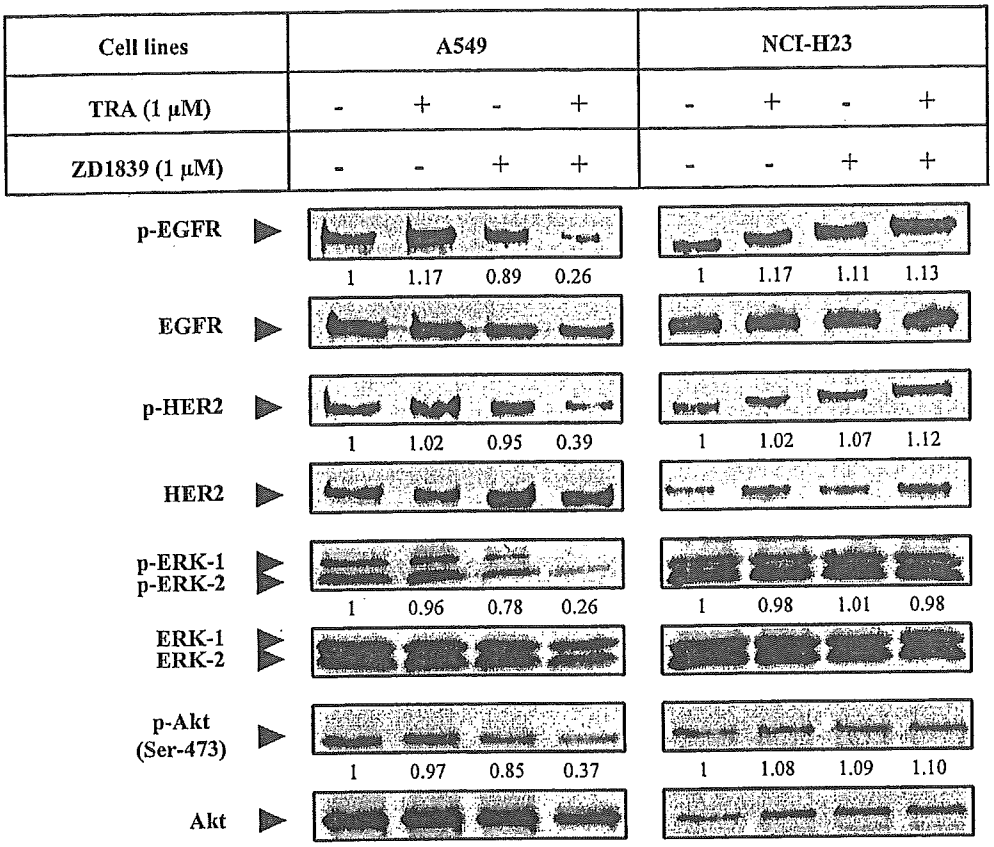

Fig. 5. Effects of combination treatment with ZD1839 and trastuzumab (TRA) on intracellular signaling molecules. The effects on EGFR, HER2, ERK-1/2, and Akt were examined in drug-sensitive A549 and drug-resistant NCI-H23 cells. Cells were treated for 3 h with ZD1839 at 1 μM and/or TRA at 1 μM. Equal amounts of protein were separated by SDS-PAGE and probed with the antibodies indicated, as detailed in Section 2. EGFR, HER2, ERK-1/2, and Akt activity were determined using the corresponding anti-phospho antibodies. EGFR, HER2, ERK-1/2, and Akt protein levels were evaluated using anti-EGFR, anti-HER2, anti-ERK-1/2, and anti-Akt antibodies. Similar results were obtained in repeated experiments. Values indicate the density of the bands.

no effects at all on the other NSCLC cell lines examined. A549 cells treated with both ZD1839 and trastuzumab under basal growth conditions showed an increased number of cells at G_0/G_1 phase, increased p27 expression, decreased expression of cyclin E and cyclin D1, and decreased Rb phosphorylation compared with cells treated with either drug on its own. Combination treatment reduced the phosphorylation of EGFR, HER2, ERK-1/2, and Akt compared with treatment with either agent alone.

Anido et al. [43] demonstrated that ZD1839 induced the formation of inactive EGFR/HER2 and EGFR/HER3 heterodimers in breast cancer cells under basal growth conditions. In the present study, EGFR/HER2 heterodimers were detected in ZD1839-sensitive A549 cells, but not in ZD1839-resistant NCI-H23 cells, under basal growth conditions. Heterodimer formation might be necessary for sensitivity to growth inhibition induced by ZD1839 or a combination of ZD1839 and trastuzumab. Consistent with the results of Anido et al. [43], we found that ZD1839 induced a increase in EGFR/HER2 heterodimer formation in A549 cells. We therefore suggest that inactive heterodimers, which block EGFR and HER2-induced signaling, are formed, in the presence of ZD1839. A recent highlight is finding that either therapeutic efficacy of ZD1839 or drug sensitivity to ZD1839 is closely associated with somatic mutations in EGFR catalytic kinase domain (mainly in exon 19 and 20)

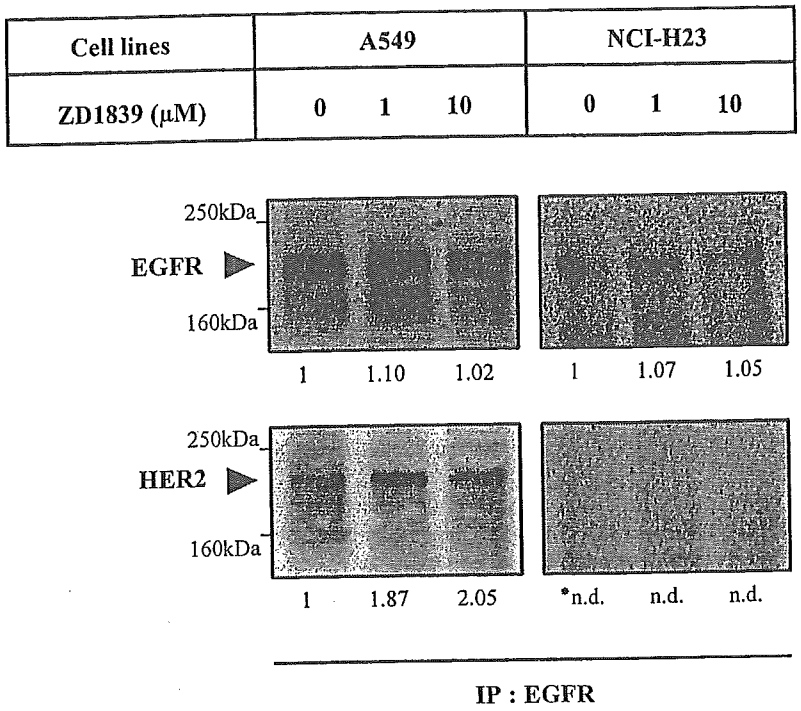

Fig. 6. Effects of ZD1839 on tile formation of EGFR/HER2 heterodimers. Cells were treated with the concentrations of ZD1839 indicated for 3 h. Equal amounts of protein were then subjected to immunoprecipitation using anti-EGFR antibody. The immunoprecipitates were subjected to SDS-PAGE electrophoresis and immunoblot analysis with anti-EGFR and anti-HER2 antibodies, as detailed in Section 2. Similar results were obtained in repeated experiments. Values indicate the density of the bands. *n.d., not determined.

in NSCLC [46,47]. We have reported that cellular ZD1839 sensitivity in NSCLC cells depends upon how cellular growth and survival could be closely associated with EGF-EGFR signaling in each NSCLC cell lines [42], and also that the most ZD1839 sensitive NSCLC cell lines, PC9 cells, has deletion mutation in the EGFR catalytic kinase domain (Ono, unpublished data). In the present study, we observed no apparent mutation in exon 19 and 21 in the EGFR gene in A549 cells, a most ZD1839-sensitive cell lines in the four NSCLC cell lines examined (Nakamura and Ono, unpublished data). HER2 is often overexpressed in various malignancies including breast cancer and lung cancer. Interestingly, Stephens et al. [48] demonstrated some mutations in the gene encoding the transmembrane protein tyrosine kinase of HER2 when 120 primary lung tumors were examined. Mutation of HER2 might be important for limitation of drug sensitivity. Therefore, further study should be required to determine whether any mutation of HER2 could be associated with therapeutic efficacy combination therapy. It is also very important to determine whether phosphorylation of EGFR and HER2 could affect their interaction. We demonstrated that combination treatment with ZD1839 and trastuzumab showed significant inhibition of phosphorylation of EGFR and HER2 in A549 cells (Fig. 5). Anido et al. [43] reported that ZD1839 did not induce the formation of inactive EGFR/HER2 heterodimers but inhibit the phosphorylation of EGFR/HER2 heterodimers in breast cancer cells. Combination treatment may be accompanied by reduced phosphorylation of EGFR/HER2 heterodimers with increased EGFR/HER2 heterodimer formation.

Animal experiments using xenografts of breast cancer and other epithelial tumor cells have revealed that tumors that overexpress HER2 show the greatest sensitivity to ZD1839 [35,36]. Several reports have found that EGFR levels are not directly, correlated with the sensitivity of cancer cells to ZD1839 [20,23, 42,49,50]. In the present study, three of the four

NSCLC cell lines examined (A549, NCI-H23, and NCI-H727) expressed comparable levels of EGFR, whereas A549 and NCI-H23 cells showed relatively higher and lower sensitivity to growth inhibition by ZD1839, respectively. A549 and NCI-H661 cells expressed HER2 protein at comparable levels. Therefore, sensitivity to ZD1839 did not seem to be directly associated with either EGFR or HER2 protein levels, which was consistent with the results of previous studies [42,43,46]. Ono et al. [42] reported that the expression levels of EGFR and HER2 in A431 cells were 33-fold and 1.07-fold higher than A549 cells. On the other hand, Janmaat et al. [50] reported that the expression levels of EGFR and HER2 in A431 cells were 7.5-fold and 1.3-fold higher than A549 cells. We demonstrated that the expression levels of EGFR and HER2 in A431 cells were 2.9-fold and 1.56-fold higher than A549 cells. Experimental conditions to evaluate the value of relative expression of EGFR and HER2 were somewhat different in these studies: protein expression levels by Western blot (Ono et al. and our present study) and protein expression levels by flow cytometry (Janmaat et al.). Moreover, we analyzed with 10 μg protein of cell lysates from each cell lines, while Ono et al. used 100 μg protein of cell lysates for each assays. The potential reasons for such differences might be probably due to different experimental condition used in these studies.

In our recent study involving nine different NSCLC cell lines, we proposed that sensitivity to ZD1839 might be associated with the dependence of cells on ERK-1/2 and Akt activation in response to EGFR signaling for proliferation and survival [42]. In the present study, the A549 cell line showed significantly greater sensitivity not only to ZD1839 but also to a combination of ZD1839 and trastuzumab,

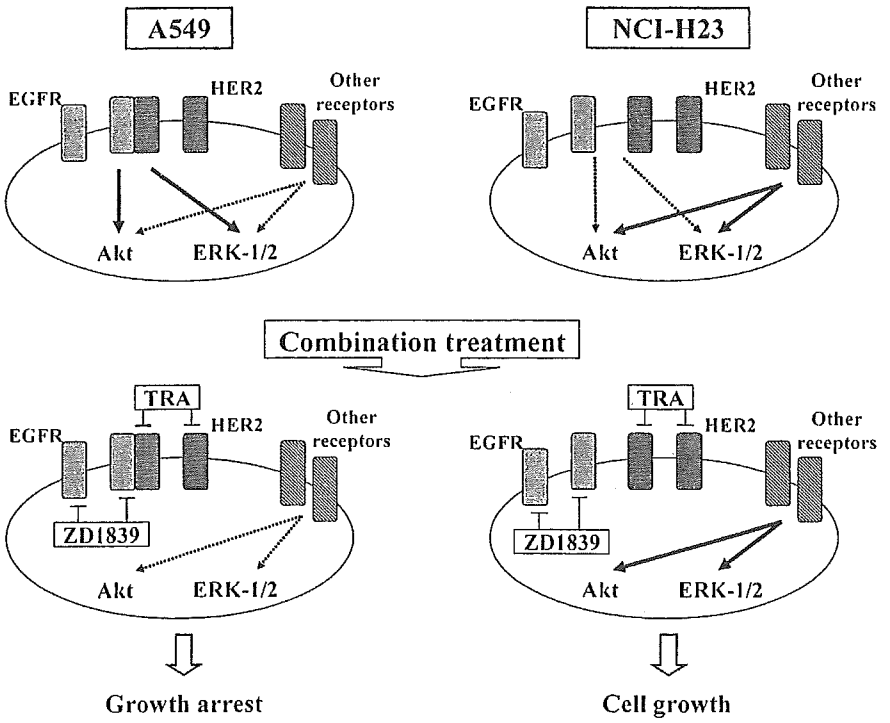

Fig. 7. A model of the growth-inhibitory response of NSCLC cells to combined ZD1839 and trastuzumab (TRA) treatment. The combination treatment-sensitive A549 cells are driven by EGFR/HER2 heterodimers and EGFR and/or HER2. The activation of ERK-1/2 and Akt in response to EGFR and HER2 signaling, which is essential for cell proliferation and survival, is blocked by ZD1839 and/or TRA. By contrast, in the combination treatment-resistant NCI-H23 cells, EGFR/HER2 heterodimers and EGFR and/or HER2 are not essential, and other factors or receptors drive cell growth following activation by downstream signaling effectors. Therefore, combination treatment that targets EGFR/HER2 heterodimers inhibits signal transduction and cell-cycle progression in the sensitive NSCLC cell lines.

compared with the other cell lines examined. By contrast, the NCI-H23 cell line showed reduced sensitivity to ZD1839 both alone and in combination with trastuzumab. These findings indicate that the high sensitivity of A549 cells to a combination of ZD1839 and trastuzumab is closely correlated with dependence on ERK-1/2 and Akt activation in response to both EGFR and HER2 signaling for proliferation and survival. Furthermore, this process appears to involve EGFR/HER2 heterodimers (Fig. 7). No EGFR/HER2 heterodimers were formed in the NCI-H23 cells, resulting in a much lower sensitivity to growth inhibition induced by a combination of ZD1839 and trastuzumab.

In conclusion, we have demonstrated significant growth inhibition in cultured NSCLC cells induced by combination treatment with the EGFR-targeting drug ZD1839 and the HER2-targeting drug trastuzumab. This combination might have improved therapeutic efficacy against advanced NSCLC cells expressing both EGFR and HER2. Further studies with animal models will be necessary to confirm the effectiveness of this novel therapeutic strategy against NSCLC.

Acknowledgements

We thank Akira Hirata (Kyusyu University, Fukuoka, Japan) for fruitful discussions. This study was supported in part by a Grant-in-Aid for Cancer Research from the Ministry of Education, Culture, Sports, Science and Technology, Japan, and the Ministry of Health, Labor and Welfare, Japan.

References

[1] J. Mendlsohn, J. Baserga, The EGF receptor family as targets for cancer therapy, Oncogene 19 (2000) 6550–6565.
[2] J.S. de Bono, E.K. Rowinsky, The ErbB receptor family: a therapeutic target for cancer, Trends Mol. Med. 8 (2002) 19–26.
[3] J.R. Woodburn, The epidermal growth factor receptor and its inhibition in cancer therapy, Pharmacol. Ther. 82 (1999) 241–250.
[4] M.A. Olayioye, R.M. Neve, H.A. Lane, The ErbB signaling network: receptor heterodimerization in development and cancer, Eur. Mol. Biol. Org. J. 19 (2000) 3159–3167.
[5] D.S. Salomon, R. Brndt, F. Ciardiello, N. Normanno, Epidermal growth factor-related peptides and their receptors in human malignancies, Crit. Rev. Oncol. Hematol. 19 (1995) 183–232.
[6] C.L. Arteaga, Epidermal growth factor receptor dependence in human tumors: more than just expression, Oncologist 7 (2002) 31–39.
[7] K. Khazaie, V. Schirrmacher, R.B. Lichtner, EGFR receptor in neoplasia and metastasis, Cancer Metastasis Rev. 12 (1993) 255–274.
[8] E. Raymond, S. Faivre, J.P. Armand, Epidermal growth factor receptor tyrosine kinase as a target for anticancer therapy, Drugs 60 (2000) 15–23.
[9] D. Graus-Porta, R.R. Beerli, J.M. Daly, N.E. Hynes, ErbB-2, the preferred heterodimerization partner of all ErbB receptors, is a mediator of lateral signaling, Eur. Mol. Biol. Org. J. 16 (1997) 1647–1655.
[10] D. Karunagaran, E. Tzahar, R.R. Beerli, ErbB-2 is a common auxiliary subunit of NDF and EGF receptors: implications for breast cancer, Eur. Mol. Biol. Org. J. 15 (1996) 254–264.
[11] K.S. Spencer, D. Graus-Porta, J. Leng, ErbB2 is necessary for induction of carcinoma cell invasion by ErbB family receptor tyrosine kinases, J. Cell Biol. 148 (2000) 385–397.
[12] J.R. Sainsbury, J.R. Farndon, G.K. Needham, A.J. Malcolm, A.L. Harris, Epidermal-growth-factor receptor status as predictor of early recurrence of and death from breast cancer, Lancet 1 (1987) 1398–1402.
[13] J. Brabender, K.D. Danenberg, R. Metzger, P.M. Schncider, J. Park, D. Salonga, et al., Epidermal growth factor receptors and HER2-neu mRNA expression in non-small cell lung cancer is correlated with survival, Clin. Cancer Res. 7 (2001) 1850–1855.
[14] D. Veale, N. Kerr, G.J. Gibson, P.J. Kelly, A.L. Harris, The relationship of quantitive epidermal growth factor receptor expression in non-small cell lung cancer to long term survival, Br. J. Cancer 68 (1993) 162–165.
[15] F. Ciardiello, G. Tortora, A novel approach in the treatment of cancer: targeting the epidermal growth factor receptor, Clin. Cancer Res. 7 (2001) 1958–1970.
[16] J. Baselga, S.D. Averbuch, ZD1839 ('Iressa') as an anticancer agent, Drugs 60 (2000) 33–40.
[17] J.B. Gibbs, Anticancer drug targets: growth factors and growth factor signaling, J. Clin. Invest. 105 (2000) 9–13.
[18] S.B. Noonberg, C.C. Benz, Tyrosine kinase inhibitors targeted to the epidermal growth factor receptor subfamily: role as anticancer agents, Drugs 59 (2000) 753–767.
[19] A.E. Wakeling, A.J. Barker, D.H. Davies, D.S. Brown, L.R. Green, S.A. Cartidge, et al., Specific inhibition of epidermal growth factor receptor tyrosine kinase by 4-anilinoquinazolines, Breast Cancer Res. Treat. 38 (1996) 67–73.
[20] F. Ciardiello, R. Caputo, R. Bianco, V. Damiano, G. Pomatico, S. De Placido, et al., Antitumor effect and potentiation of cytotoxic drugs activity in human cancer cells by ZD1839 (Iressa), an epidermal growth factor receptor-selective tyrosine kinase inhibitor, Clin. Cancer Res. 6 (2000) 2053–2063.

[21] F. Ciardiello, R. Caputo, R. Bianco, V. Damiano, G. Fontanini, S. Caccato, et al., Inhibition of growth factor production and angiogenesis in human cancer cells by ZD1839 (Iressa), a selective epidermal growth factor receptor tyrosine kinase inhibitor, Clin. Cancer Res. 7 (2001) 1459–1465.

[22] A.E. Wakeling, S.P. Guy, J.R. Woodburn, S.E. Ashton, B.J. Curry, A.J. Barker, et al., ZD1839 (Irresa): an orally active inhibitors of epidermal growth factor signaling with potential for cancer therapy, Cancer Res. 62 (2002) 5749–5754.

[23] F.M. Sirotnak, M.F. Zakowski, V.A. Miller, H.I. Scher, M.G. Kris, Efficacy of cytotoxic agents against human tumor xenografts is markedly enhanced by coadministration of ZD1839 (Iressa), a inhibitor of EGFR tyrosine kinase, Clin. Cancer Res. 6 (2000) 4885–4892.

[24] Y. Nishiwaki, J. Yansteenkiste, S. Kudoh, A multi-institutional randomized phase II trial of gefitinib for previously treated patients with advanced non-small-cell lung cancer (the IDEAL 1 trial), J. Clin. Oncol. 21 (2003) 2237–2241.

[25] M. Kris, R.B. Natale, R. Herbst, A phase II trial of ZD1839 ('Iressa') in advanced non-small cell lung cancer (NSCLC) patients who had failed platinum- and docetaxel-based regimens (IDEAL 2), Proc. Am. Soc. Clin. Oncol. 21 (2002) 292.

[26] J. Baselga, Targeting the epidermal growth factor receptor-tyrosine kinase inhibitors: small molecules, big hopes, J. Clin. Oncol. 20 (2002) 2217–2219.

[27] M. Fukuoka, S. Yano, G. Giaccone, T. Tamura, K. Nakagawa, J.Y. Douillard, et al., Multi-institutional randomized phase II trial of gefitinib for previously treated patients with advanced non-small-cell lung cancer, J. Clin. Oncol. 21 (2003) 2237–2246.

[28] H.M. Shepard, G.D. Lewis, J.C. Sarup, Monoclonal antibody therapy of human cancer: taking the HER2 protooncogene to the clinic, J. Clin. Immunol. 11 (1991) 117–127.

[29] R. Colomer, R. Lupu, S.S. Bacus, E.P. Gelmann, ErbB-2 antisense oligonucleotides inhibit the proliferation of breast carcinoma cells with ErbB-2 oncogene amplification, Br. J. Cancer 70 (1994) 819–825.

[30] X. Liu, B.G. Pogo, Inhibition of ErbB-2-positive breast cancer cell growth by ErbB-2 antisense oligonucleotides, Antisense Nucleic Acid Drug Dev. 6 (1996) 9–16.

[31] H. Roh, J. Pippin, J.A. Drebin, Down-relgulation of HER2/neu expression induces apoptosis in human cancer cells that overexpress HER2/neu, Cancer Res. 60 (2000) 560–565.

[32] J. Baselga, D. Tripathy, J. Mendelsohn, Phasa II study of weekly intravenous recombinant humanized anti-p185HER2 monoclonal antibody in patients with HER2/neu-overexpressing metastatic breast cancer, J. Clin. Oncol. 14 (1996) 737–744.

[33] M.D. Pegram, A. Lipton, D.F. Hayes, Phase II study of receptor-enhanced chemosensitivity using recombinant humanized anti-p185HER2/neu monoclonal antibody plus cisplatin in patients with HER2/neu-overexpressing metastatic breast cancer refractory to chemotherapy treatment, J. Clin. Oncol. 16 (1998) 2659–2671.

[34] T. Tamura, Moleclular target-based cancer therapy: epidermal growth factor receptor inhibitors, Jpn. J. Surg. 2 (2002) 233–236.

[35] M.M. Moasser, A. Basso, S.D. Averbuch, N. Rosen, The tyrosine kinase inhibitor ZD1839 ('Iressa') inhibits HER2-driven signaling and suppresses the growth of HER2-over-expressing tumor cells, Cancer Res. 61 (2001) 7184–7188.

[36] S.L. Moulder, F.M. Yakes, S.K. Muthuswamy, J.F. Simpson, C.L. Arteaga, Epidermal growth factor receptor (HER1) tyrosine kinase inhibitor ZD1839 (Irresa) inhibits HER2/neu (erbB2)-overexpressing breast cancer cells in vitro and in vivo, Cancer Res. 61 (2001) 8887–8895.

[37] N. Normanno, M. Campiglio, A. De Luca, G. Somenzi, M. Maiello, F. Ciardiello, et al., Cooperative inhibitory effect of ZD1839 (Iressa) in combination with trastuzumab (Herceptin) on human breast cancer cell growth, Ann. Oncol. 13 (2002) 65–72.

[38] J. Anido, J. Albanell, F. Rojo, J. Codony-Servat, J. Arribas, J. Baselga, Inhibition by ZD1839 (Iressa) of epidermal growth factor (EGF) and heregulin induced signaling pathways in human breast cancer cells, Proc. Am. Soc. Clin. Oncol. 20 (2001) 1712A.

[39] A.L. Harris, S. Nicholson, J.R. Sainsbury, J. Farndon, C. Wright, Epidermal growth factor receptors in breast cancer: association with early relapse and death, poor response to hormones and interactions with neu, J. Steroid Biochem. 34 (1989) 123–131.

[40] A. Osaki, M. Toi, H. Yamada, Prognostic significance of co-expression of c-ErbB-2 oncoprotein and epidermal growth factor receptor in breast cancer patients, Am. J. Surg. 164 (1992) 323–326.

[41] A. Harlozninska, J.K. Bar, R. Wenderski, M. Bebenek, Relationship between c-ErbB-2 oncoprotein, epidermal growth factor receptor, and estrogen receptor expression in patients with ductal breast carcinoma. Association with tumor phenotypes, In Vivo 10 (1996) 217–222.

[42] M. Ono, A. Hirata, T. Kometani, M. Miyagawa, S. Ueda, H. Kinoshita, et al., Sensitivity to gefitinib (Iressa, ZD1839) in non-small cell lung cancer cell lines correlates with dependence on the epidermal growth factor (EGF) receptor/extracellular signal-regulated kinase 1/2 and EGF receptor/Akt pathway for proliferation, Mol. Cancer Ther. 3 (2004) 465–472.

[43] J. Anido, P. Matar, J. Albanell, G. Marta, F. Rojo, J. Arribas, et al., ZD1839, a specific epidermal growth factor receptor (EGFR) tyrosine kinase inhibitor, induces the formation of inactive EGFR/HER2 and EGFR/HER3 heterodimers and prevents heregulin signaling in HER2-overexpressing breast cancer cells, Clin. Cancer Res. 9 (2003) 1274–1283.

[44] N.G. Aderson, T. Ahmad, K. Chan, R. Dobson, N.J. Bundred, ZD1839 (Iressa), a novel epidermal growth factor receptor (EGFR) tyrosine inhibitor, potently inhibits the growth of EGFR-positive cancer cell lines with or without ErbB2 overexpression, Int. J. Cancer 94 (2001) 774–782.

[45] D. Ye, J. Mendelsohn, Z. Fan, Augmentation of a humanized anti-HER2 monoclonal antibody 4D5 induced growth inhibition by a human-mouse chimeric anti-EGF receptor monoclonal antibody C225, Oncogene 18 (1999) 731–738.

[46] T.J. Lynch, D.W. Bell, R. Sordella, S. Gurubhagavatula, R.A. Okimoto, B.W. Brannigan, et al., Activating mutations in the epidermal growth factor receptor underlying responsiveness of non-small-cell lung cancer to gefitinib, N. Engl. J. Med. 350 (2004) 2129–2139.

[47] J.G. Paez, P.A. Janne, J.C. Lee, S. Tracy, H. Greulich, S. Gabriel, et al., EGFR mutations in lung cancer: correlation with clinical response to gefitinib therapy, Science 304 (2004) 1497–1500.

[48] P. Stephens, C. Hunter, G. Bignell, S. Edkins, H. Davies, J. Teague, et al., Lung cancer: intragenic ERBB2 kinase mutations in tumors, Nature 431 (2004) 525–526.

[49] T. Suzuki, T. Nakagawa, H. Endo, T. Mitsudomi, A. Masuda, Y. Yatabe, et al., The sensitivity of lung cancer cell lines to the EGFR-selective tyrosine kinase inhibitor ZD1839 ('Iressa') is not related to the expression of EGFR or HER-2 or to K-ras gene status, Lung Cancer 42 (2003) 35–41.

[50] M.L. Janmaat, F.A.E. Kruyt, J.A. Rodriguez, G. Giaccone, Response to epidermal growth factor receptor inhibits in non-small cell lung cancer cells: limited antiproliferative effects and absence of apoptosis associated with persistent activity of extracellular signal-regulated kinase or Akt kinase pathways, Clin. Cancer Res. 9 (2003) 2316–2326.

Infiltration of COX-2–expressing macrophages is a prerequisite for IL-1β–induced neovascularization and tumor growth

Shintaro Nakao,[1,2] Takashi Kuwano,[1] Chikako Tsutsumi-Miyahara,[2] Shu-ichi Ueda,[1] Yusuke N. Kimura,[3,4] Shinjiro Hamano,[5] Koh-hei Sonoda,[2] Yasuo Saijo,[6] Toshihiro Nukiwa,[6] Robert M. Strieter,[7] Tatsuro Ishibashi,[2] Michihiko Kuwano,[3,4] and Mayumi Ono[1,3]

[1]Department of Medical Biochemistry, [2]Department of Ophthalmology, Graduate School of Medical Sciences, and [3]Collabo-Station II, Kyushu University, Fukuoka, Japan. [4]Research Center of Innovative Cancer Therapy, Kurume University, Kurume, Japan. [5]Department of Parasitology, Graduate School of Medical Sciences, Kyushu University, Fukuoka, Japan. [6]Department of Respiratory Oncology and Molecular Medicine, Institute of Development, Aging, and Cancer, Tohoku University, Sendai, Japan. [7]Department of Medicine, Division of Pulmonary and Critical Care Medicine, David Geffen School of Medicine, University of California at Los Angeles, Los Angeles, California, USA.

Inflammatory angiogenesis is a critical process in tumor progression and other diseases. The inflammatory cytokine IL-1β promotes angiogenesis, tumor growth, and metastasis, but its mechanisms remain unclear. We examined the association between IL-1β–induced angiogenesis and cell inflammation. IL-1β induced neovascularization in the mouse cornea at rates comparable to those of VEGF. Neutrophil infiltration occurred on day 2. Macrophage infiltration occurred on days 4 and 6. The anti–Gr-1 Ab-induced depletion of infiltrating neutrophils did not affect IL-1β– or VEGF-induced angiogenesis. The former was reduced in monocyte chemoattractant protein-1–deficient (MCP-1$^{-/-}$) mice compared with wild-type mice. After day 4, clodronate liposomes, which kill macrophages, reduced IL-1β–induced angiogenesis and partially inhibited VEGF-induced angiogenesis. Infiltrating macrophages near the IL-1β–induced neovasculature were COX-2 positive. Lewis lung carcinoma cells expressing IL-1β (LLC/IL-1β) developed neovasculature with macrophage infiltration and enhanced tumor growth in wild-type but not MCP-1$^{-/-}$ mice. A COX-2 inhibitor reduced tumor growth, angiogenesis, and macrophage infiltration in LLC/IL-1β. Thus, macrophage involvement might be a prerequisite for IL-1β–induced neovascularization and tumor progression.

Introduction

Angiogenesis, which involves a balance of promoters and inhibitors, is enhanced in many diseases (1). However, clinical trials with antiangiogenic factors have been less effective than predicted from mouse models, suggesting angiogenesis may be orchestrated by a more complex set of growth factors, cytokines, and cell types (2).

IL-1β is an inflammatory cytokine that might modulate angiogenesis by directly interacting with vascular endothelial cells or enhancing the production of proangiogenic factors via paracrine control (3–5). IL-1β stimulates endothelial cell migration and proliferation, adhesion-molecule expression, inflammatory mediator production, and leukocyte recruitment. It is required for tumor growth, metastasis, and angiogenesis in several animal models (6–8). IL-1β receptor antagonists inhibit angiogenesis and tumor development, suggesting that IL-1β receptor signaling is involved in inflammation and tumor growth (9). Song et al. reported that IL-1α reduced tumorigenicity by inducing antitumor immunity, while IL-1β promoted invasiveness, tumor angiogenesis, and host immune suppression (10).

During inflammation, vessel formation allows the rapid influx of nutrients and inflammatory cells, supplying key cytokines and growth factors to the angiogenic bed. Neutrophils, which modulate the host immune response, appear during angiogenesis induced by corneal injury or bFGF (11) and produce several proangiogenic cytokines. Monocytes, which differentiate into macrophages, migrate to inflammatory sites in response to chemotactic factors (12). Monocyte chemoattractant protein-1–deficient (MCP-1$^{-/-}$) mice that cannot recruit monocytes are resistant to experimental autoimmune encephalomyelitis and display delayed wound re-epithelization (13–15). Activated macrophages function in pathological hemangiogenesis and lymphangiogenesis in choroidal neovascularization, in advanced atherosclerosis and inflammation, and in malignant tumor development (16–19). Macrophages in the tumor stroma are closely correlated with neovascularization and poor prognosis in human cancers, including breast (20, 21), glioma (22), prostate (23), cervix (24, 25), lung (26), bladder (27), and melanoma (5, 28). Activated macrophage infiltration might influence the angiogenesis cascade by producing growth stimulators and inhibitors, cytokines, and proteolytic enzymes (20, 29, 30). However, it remains unclear how infiltrating macrophages function in angiogenesis and tumor enlargement along with the inflammatory response.

We previously demonstrated that IL-1β induced angiogenesis in vitro and in vivo through the COX-2–prostanoid pathway (31).

Nonstandard abbreviations used: Cl_2MDP-LIP, clodronate liposome; CXCL1, CXC chemokine ligand 1; CXCR2, CXC chemokine receptor 2; DFU, 5,5-dimethyl-3-(3-fluorophenyl)-4-(4-methylsulphonyl)phenyl-2((5)H)-furanone; ENA-78, epithelial neutrophil-activating peptide-78; LLC, Lewis lung carcinoma; LLC/IL-1β, LLC cells expressing IL-1β; LLC/neo, LLC cells expressing *neo*^{R}; MCP-1, monocyte chemoattractant protein-1; MIP-2, macrophage inflammatory protein 2; PBS-LIP, PBS-containing liposome; s.c., subconjunctival(ly); TXA_2, thromboxane A_2.

Conflict of interest: The authors have declared that no conflict of interest exists.

Citation for this article: *J. Clin. Invest.* **115**:2979–2991 (2005). doi:10.1172/JCI23298.

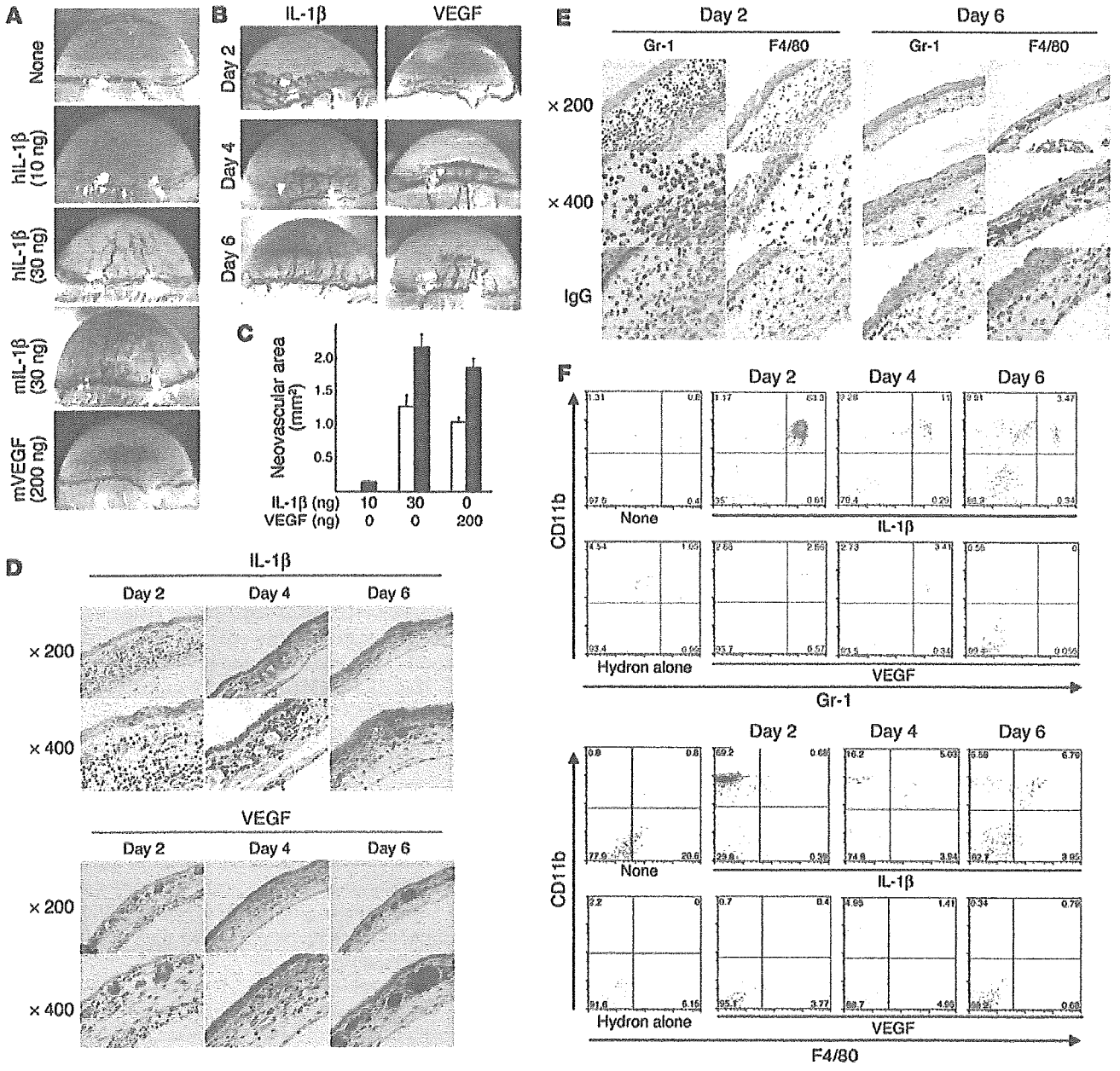

Figure 1

IL-1β– and VEGF-induced angiogenesis and inflammatory cell infiltration in mouse corneas. (**A**) Neovascularization 6 days after implanting Hydron pellets containing human or mouse IL-1β or mouse VEGF at the doses shown into male BALB/c mouse corneas. hIL-1β, human IL-1β; mIL-1β, mouse IL-1β; mVEGF, mouse VEGF. (**B**) Corneal neovascularization induced by human IL-1β (30 ng) or mouse VEGF (200 ng) at the indicated time points. (**C**) Quantitative analysis of neovascularization on days 4 (white bars) and 6 (black bars). Areas are expressed in mm^2. Bars show the mean ± SD of independent experiments (n = 6 or 7). (**D**) Corneas implanted with IL-1β or VEGF stained by H&E at the indicated time points. (**E**) Corneal sections on days 2 or 6 after IL-1β–pellet implantation, labeled immunohistochemically (brown) for Gr-1, which was detected in infiltrating cells on days 2 and 6, and F4/80, which was detected on day 6. (**F**) FACS analysis of infiltrating cells from IL-1β– or VEGF-implanted corneas (n = 5) at the indicated times. Cells were stained with PE-CD11b mAb and FITC–Gr-1 or FITC-F4/80 mAb. The percentages of infiltrating $CD11b^+Gr\text{-}1^+$ cells in IL-1β–implanted corneas were 53.5% ± 10.4% (day 2), 15.8% ± 4.9% (day 4), and 3.15% ± 0.27% (day 6). The percentages of infiltrating $CD11b^+Gr\text{-}1^+$ cells in VEGF-implanted corneas were 2.99% ± 1.37% (day 2), 1.95% ± 0.75% (day 4), and 1.08% ± 0.74% (day 6). The percentages of infiltrating $CD11b^+F4/80^+$ cells in IL-1β–implanted corneas were 1.85% ± 1.28% (day 2), 5.56% ± 1.61% (day 4), and 5.52% ± 1.14% (day 6). The percentages of infiltrating $CD11b^+F4/80^+$ cells in VEGF-implanted corneas were 0.81% ± 0.47% (day 2), 1.30% ± 1.03% (day 4), and 1.90% ± 0.98% (day 6).

Several reports showed that IL-1β enhanced tumor growth and metastasis via angiogenesis along with inflammatory cell infiltration around cancer cells (6, 8). We observed the infiltration of COX-2–positive cells around IL-1β–induced neovasculature (31). The current study investigated how IL-1β–induced angiogenesis was coordinated with the infiltration of inflammatory cells.

Results

IL-1β–induced angiogenesis in mouse corneas. We implanted hydron pellets impregnated with human IL-1β, mouse IL-1β, or mouse VEGF into mouse corneas, and outgrowth of new blood vessels was observed 6 days later. While 10 ng human IL-1β induced negligible angiogenesis, 30 ng human and 30 ng mouse IL-1β induced levels of angiogenesis similar to those induced by 200 ng VEGF.

We next examined corneal neovascularization induced by IL-1β or VEGF in more detail (Figure 1B). On day 2, vascular loop structures appeared in IL-1β– and VEGF-implanted corneas; the former showed greater dilation than the latter. On day 4, these structures disappeared from the IL-1β–treated corneas, and both IL-1β and VEGF induced corneal neovascularization extending halfway between the limbus and the pellets. On day 6, the corneal neovascularization reached the pellets. Quantitative analysis demonstrated that 30 ng IL-1β and 200 ng VEGF induced comparable levels of corneal neovascularization on days 4 and 6 (Figure 1C).

Infiltration of inflammatory cells into mouse corneas in response to IL-1β. We examined inflammatory cell infiltration into the cornea in response to IL-1β using histological examination (Figure 1, D and E) and flow cytometry (Figure 1F). On day 2, histological sections revealed prominent inflammatory cell infiltration and edema of the stromal layer around the neovasculature. These effects were absent after VEGF implantation. On day 6, numerous inflammatory cells were present in the IL-1β–implanted cornea whereas few were seen in the VEGF-implanted cornea (Figure 1D).

The cell types infiltrating the IL-1β–induced neovasculature in the cornea were identified using specific mAbs against neutrophils

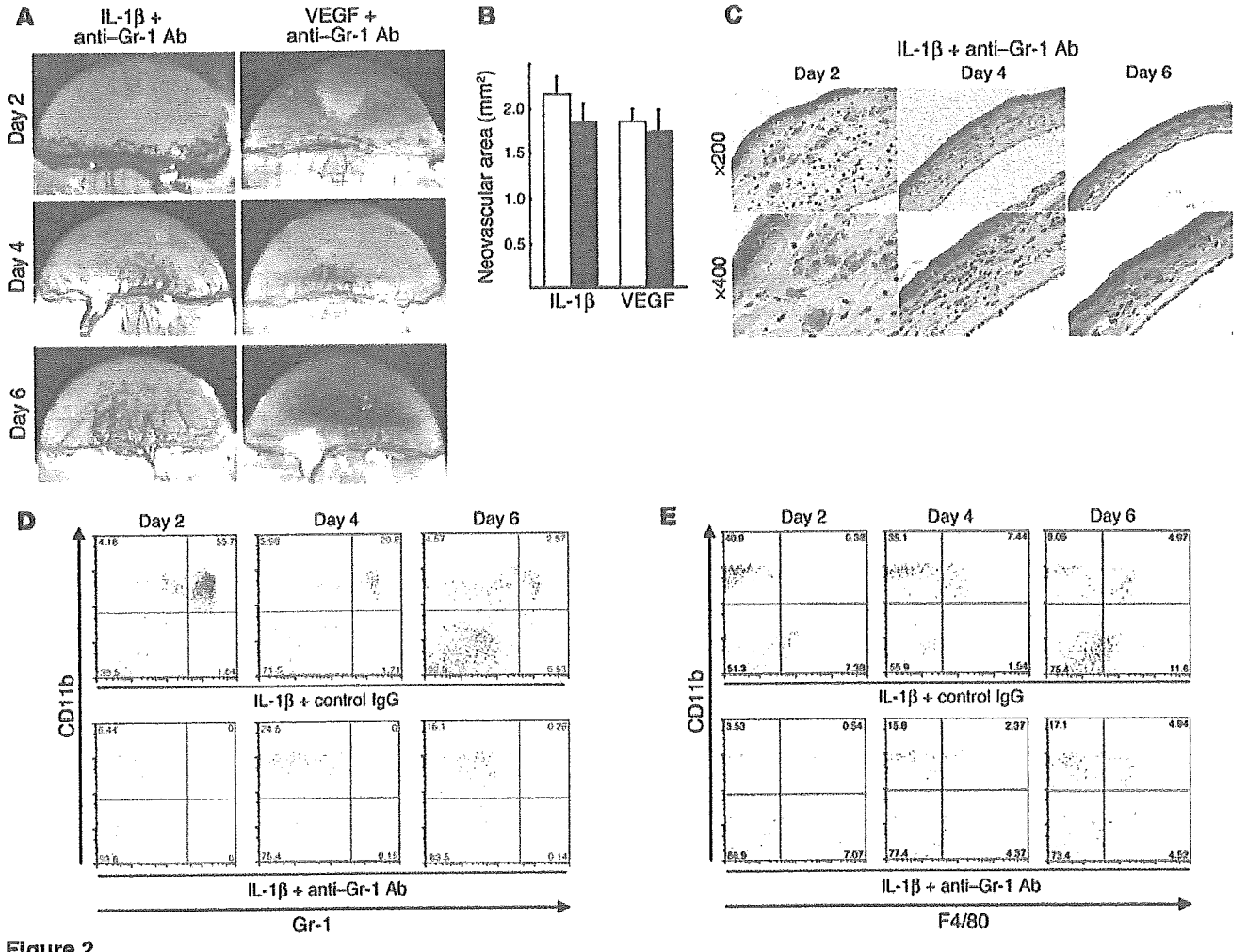

Figure 2

The role of neutrophils in IL-1β– or VEGF-induced angiogenesis. (**A**) BALB/c mice received 200 μg neutralizing anti–Gr-1 mAb i.p. on days –1, 1, 3, and 5. Hydron pellets containing IL-1β (30 ng) or VEGF (200 ng) were implanted into the corneas on day 0. Corneal vessels in the region of the pellet implants were photographed at the indicated time points. (**B**) Anti–Gr-1 mAb did not suppress IL-1β– or VEGF-induced corneal neovascularization. Corneal neovascularization 6 days after treatment with anti–Gr-1 mAb (black bars) or control IgG (white bars) was quantified by area, in mm². The bars show means ± SD of independent experiments (n = 3 or 4). (**C**) Corneas implanted with IL-1β stained by H&E at the indicated time points. Anti–Gr-1 mAb did not affect IL-1β–induced corneal edema on day 2. (**D**) FACS analysis of infiltrating cells after IL-1β implantation (n = 5) and treatment with anti–Gr-1 mAb or control IgG at the indicated times. The cells were stained with PE-CD11b mAb or FITC–Gr-1. The percentages of CD11b⁺Gr-1⁺ cells in IL-1β–implanted corneas of anti–Gr-1 mAb-treated mice were 0.25% ± 0.22% (day 2), 0.11% ± 0.1% (day 4), and 0.28% ± 0.37% (day 6). (**E**) FACS analysis of infiltrating cells from 5 IL-1β–implanted corneas treated with anti–Gr-1 mAb or control IgG at the indicated times. Cells were stained with PE-CD11b mAb or FITC-F4/80. The percentages of CD11b⁺F4/80⁺ cells in IL-1β–implanted corneas of anti–Gr-1 mAb-treated mice were 1.71% ± 1.04% (day 2), 4.36% ± 1.20% (day 4), and 5.57% ± 1.34% (day 6).

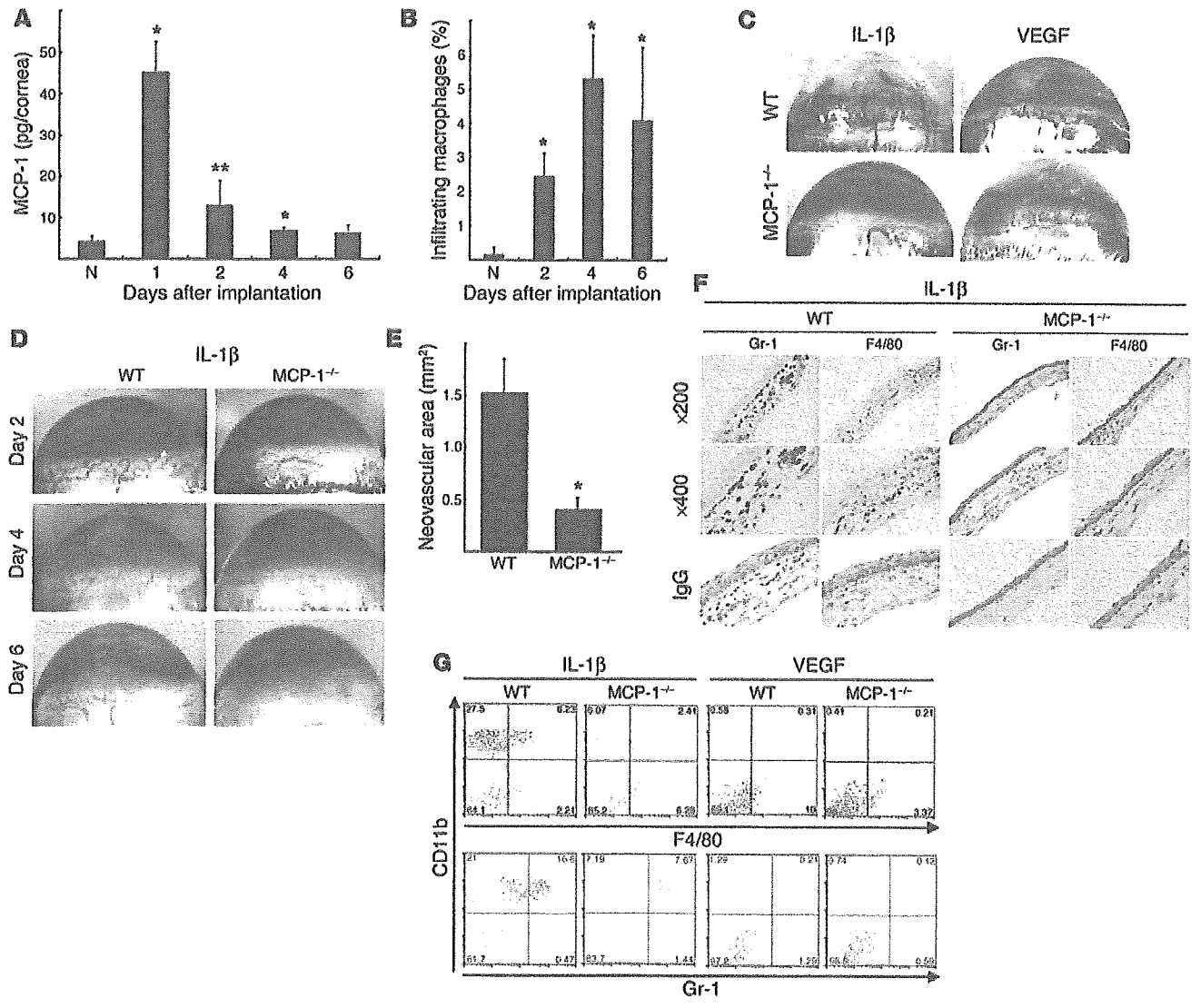

Figure 3

The role of MCP-1 in IL-1β– or VEGF-induced angiogenesis. (**A**) Kinetics of MCP-1 levels after pellet implantation. Corneal lysates were prepared and assayed by ELISA at the indicated times ($n = 3$). $^*P < 0.01$ and $^{**}P < 0.03$ versus untreated (N). (**B**) Kinetics of infiltrating macrophages in IL-1β–implanted corneas. Corneal lysates were prepared from untreated and IL-1β–treated corneas on the days shown ($n = 3$). Percentages of infiltrating F4/80$^+$ cells were quantified using FACS. (**C**) Corneal neovascularization induced by IL-1β (30 ng) or VEGF (200 ng) in C57BL/6 wild-type and MCP-1$^{-/-}$ mice on day 6. (**D**) Corneal neovascularization at the indicated time points. (**E**) Quantitative analysis of IL-1β–induced corneal neovascularization in MCP-1$^{-/-}$ ($n = 10$) and wild-type mice ($n = 8$) on day 6. Bars show means ± SD. $^*P < 0.01$ versus wild-type mice using the unpaired Student's *t* test. (**F**) Immunohistochemistry for Gr-1 or F4/80 (brown) in corneal sections on day 6 after IL-1β pellet implantation in MCP-1$^{-/-}$ or wild-type mice. Gr-1–positive cells were detected in both types of mice. F4/80-positive cells were detected on day 6 in wild-type but not MCP-1$^{-/-}$ mice. (**G**) FACS analysis of infiltrating cells from 5 IL-1β– or VEGF-implanted corneas at day 6 in wild-type or MCP-1$^{-/-}$ mice. The percentages of CD11b$^+$F4/80$^+$ cells were 4.09% ± 2.13% (IL-1β, wild-type), 2.53% ± 1.73% (IL-1β, MCP-1$^{-/-}$), 0.30% ± 0.10% (VEGF, wild-type), and 0.14% ± 0.05% (VEGF, MCP-1$^{-/-}$). The percentages of CD11b$^+$Gr-1$^+$ cells were 13.5% ± 2.89% (IL-1β, wild-type), 7.84% ± 0.48% (IL-1β, MCP-1$^{-/-}$), 0.94% ± 0.55% (VEGF, wild-type) and 0.20% ± 0.10% (VEGF, MCP-1$^{-/-}$).

(anti–Gr-1) and macrophages (anti-F4/80). On day 2, the infiltrate mainly contained neutrophils (Figure 1E) with some F4/80-positive macrophages. On day 6, numerous F4/80-positive macrophages were detected. Flow cytometry revealed that Gr-1–positive neutrophils were abundant on day 2 (53.5% ± 10.4%) but decreased on days 4 (15.8% ± 4.9%) and 6 (3.15% ± 0.27%). In contrast, F4/80-positive macrophages increased on days 4 (5.56% ± 1.61%) and 6 (5.52% ± 1.14%). There was minimal neutrophil and macrophage infiltration of control corneas implanted with hydron pellets alone (Figure 1F). There were 2- to 3-fold increases in the number of infiltrating macrophages 4 and 6 days after VEGF treatment compared with the untreated control. IL-1β induced the early infiltration of neutrophils, followed by macrophages, during angiogenesis. VEGF had weaker effects on neutrophil and macrophage infiltration.

Effect of neutrophil depletion on IL-1β–induced angiogenesis. Neutrophils were depleted by i.p.-administered anti–Gr-1 Ab in order to determine their roles in IL-1β– and VEGF-induced angiogenesis. Reduced numbers of polymorphic mononuclear cells were seen

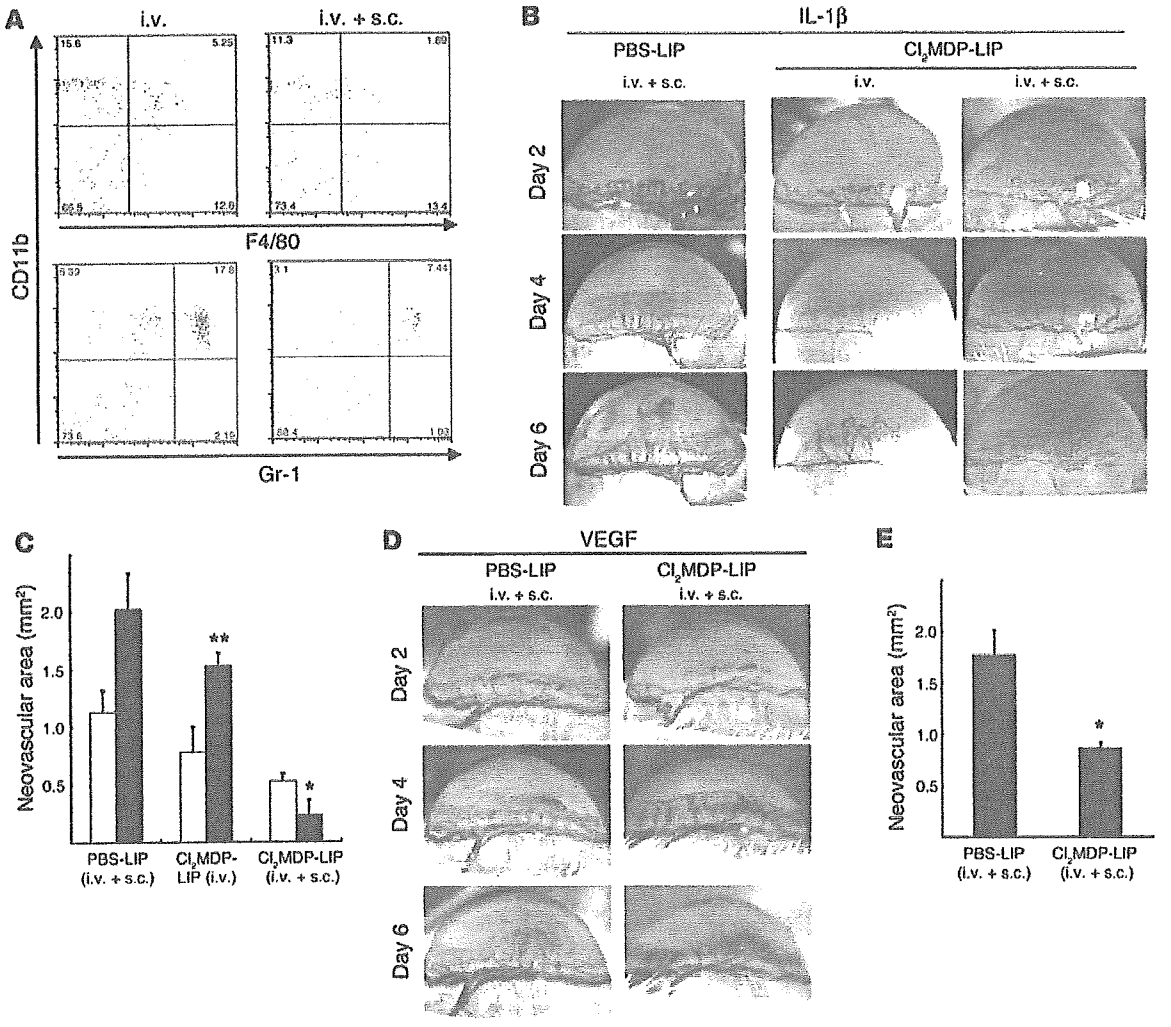

Figure 4

The effect of Cl_2MDP-LIPs on IL-1β–induced angiogenesis. (**A**) FACS analysis of infiltrating cells on day 6, in IL-1β–implanted corneas from BALB/c mice that received Cl_2MDP-LIPs or PBS-LIPs i.v. and/or s.c. The cells were stained with PE-CD11b mAb and FITC–Gr-1 or FITC-F4/80 mAb. (**B**) Corneal neovascularization at the indicated time points in BALB/c mice receiving Cl_2MDP-LIPs or PBS-LIPs i.v. and/or s.c. The percentages of infiltrating cells in IL-1β–implanted corneas of Cl_2MDP-LIP– or PBS-LIP–treated mice were 4.75% ± 0.48% (i.v., CD11b$^+$F4/80$^+$), 13.2% ± 4.03% (i.v., CD11b$^+$Gr-1$^+$), 1.63% ± 0.30% (i.v. + s.c., CD11b$^+$F4/80$^+$), and 6.61% ± 0.93% (i.v. + s.c., CD11b$^+$Gr-1$^+$). (**C**) Neovascularization was quantified by area in mm^2 on day 4 (white bars) and day 6 (black bars). Bars show means ± SD of independent experiments (n = 3 or 4; $^*P < 0.01$ and $^{**}P < 0.05$ versus PBS-LIPs). (**D**) Corneal neovascularization induced with VEGF at the indicated time points after receiving Cl_2MDP-LIPs or PBS-LIPs (i.v. + s.c.). (**E**) Quantitative analysis of neovascularization on day 6. VEGF-induced corneal neovascularization in mice (n = 6) receiving Cl_2MDP-LIPs was inhibited compared with mice (n = 6) receiving PBS-LIPs. $^*P < 0.01$ using the Student's t test.

in the peripheral blood 6 days after treatment (data not shown). Neither IL-1β– nor VEGF-induced angiogenesis was influenced by neutrophil depletion by anti–Gr-1 Ab (Figure 2, A and B). No cell infiltration was detected in IL-1β–implanted corneas treated with anti–Gr-1 Ab although edema was observed on day 2 (Figure 2C). The CD11b$^+$Gr-1$^+$ cell population was reduced by 99.5% after 2 days whereas CD11b$^+$Gr-1$^-$ and CD11b$^+$F4/80$^+$ cells persisted (Figure 2, D and E). Anti–Gr-1 Ab did not affect the appearance of F4/80-positive macrophages, suggesting neutrophil infiltration was not required for IL-1β–induced angiogenesis in mouse corneas.

IL-1β–induced angiogenesis in MCP-1$^{-/-}$ mouse corneas. The CC chemokine MCP-1 is a potent macrophage chemoattractant (12). MCP-1$^{-/-}$ mice show reduced macrophage recruitment to inflammatory sites (13–15). MCP-1 is induced by IL-1β in vitro (32), but its role in angiogenesis in vivo is unclear. ELISA showed that MCP-1 levels were significantly increased 1 day after IL-1β implantation, remained high on day 2, and were similar to those in untreated corneas on day 6 (Figure 3A). The macrophage infiltration of the IL-1β–treated corneas increased over time and peaked on day 4 (Figure 3B).

In MCP-1$^{-/-}$ mice, implanting VEGF pellets induced corneal neovascularization at levels similar to those of C57BL/6 wild-type mice (Figure 3C). In contrast, IL-1β–induced angiogenesis was reduced in MCP-1$^{-/-}$ compared with wild-type mice (Figure 3, C and D). Quantitative analysis demonstrated less IL-1β–induced corneal neovascularization in MCP-1$^{-/-}$ mice than in C57BL/6

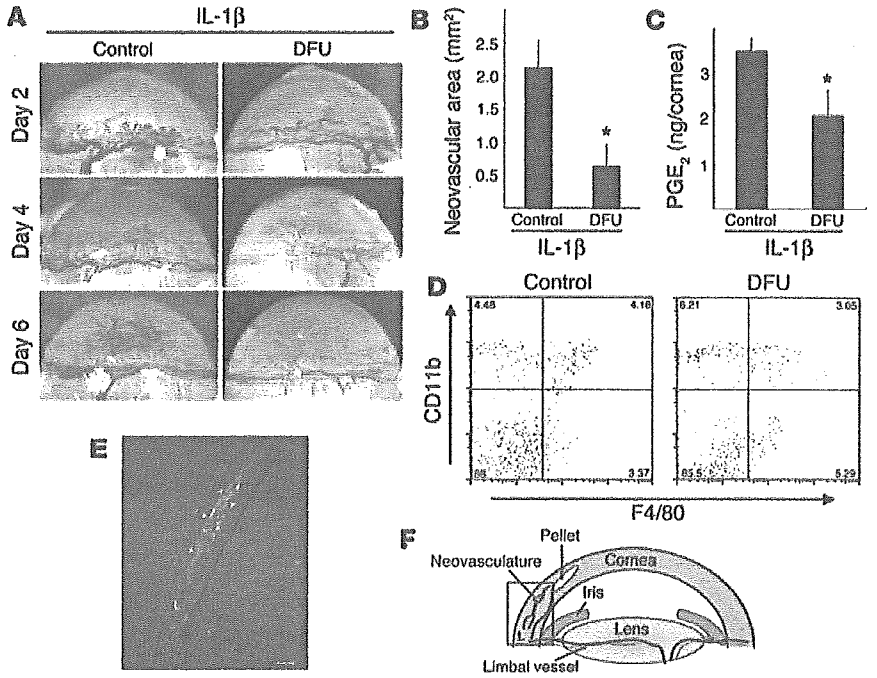

Figure 5

Expression of COX-2 in infiltrating macrophages during IL-1β–induced angiogenesis. (**A**) Corneal neovascularization on days 2, 4, and 6 in BALB/c mice receiving DFU. (**B**) Quantitative analysis of neovascularization on day 6. IL-1β–induced corneal neovascularization in mice ($n = 5$) receiving DFU was inhibited compared with control mice ($n = 7$). $^*P < 0.01$ using Student's t test. (**C**) Comparison of levels of PGE_2 in IL-1β–implanted corneas with or without DFU. On day 4, 4 IL-1β–implanted corneas of DFU-treated and untreated mice were harvested. Corneal lysates were prepared and individually assayed for PGE_2 ($n = 3$). $^{**}P < 0.05$ using Student's t test. (**D**) FACS analysis of infiltrating cells on day 6 from 5 IL-1β–implanted corneas from BALB/c mice receiving DFU and control mice. The percentages of $CD11b^+F4/80^+$ cells in mouse corneas were 4.63% ± 0.52% (control) and 3.45% ± 0.57% (DFU treated). (**E**) Representative overview of an IL-1β–implanted cornea on day 4. Arrowheads indicate infiltrated cells (yellow) that are positive for macrophage marker F4/80 (green) and COX-2 (red). L, limbus. Scale bar: 50 μm. (**F**) Corneal micropocket assay model in mice. The rectangle represents the area of the cornea used in the immunohistochemical analysis in **E**.

wild-type mice (Figure 3E). Vascular loops and sprouts typical of corneal neovascularization were present in C57BL/6 and BALB/c mice (Figures 1B and 3D). On day 2 after IL-1β treatment, vascular loops were seen in the neovasculature of MCP-$1^{-/-}$ mice. On days 4 and 6, the vessel sprouts were reduced in MCP-$1^{-/-}$ mice compared with wild-type mice. The infiltration of Gr-1–positive neutrophils into IL-1β–treated corneas of wild-type and MCP-$1^{-/-}$ mice was confirmed histologically and by flow cytometry (Figure 3, F and G). The number of Gr-1–positive neutrophils was lower in MCP-$1^{-/-}$ mice than in wild-type mice. There was less infiltration by F4/80-positive macrophages in IL-1β–treated MCP-$1^{-/-}$ mice than in IL-1β–treated wild-type mice, suggesting an important role for these cells in IL-1β–induced corneal neovascularization.

Macrophage depletion reduced IL-1β–induced angiogenesis. Clodronate liposomes (Cl_2MDP-LIPs) are phagocytosed by macrophages and induce rapid apoptosis (33, 34). Cl_2MDP-LIPs administered i.v. to mice depleted macrophages in the spleen and liver (data not shown) but not the cornea (Figure 4A) and mildly inhibited IL-1β–induced angiogenesis (Figure 4, B and C). Cl_2MDP-LIPs administered by i.v. and subconjunctival (s.c.) injection depleted macrophages in the cornea (80.5% depletion on day 6), spleen, liver, and submandibular lymph nodes (Figure 4, B and C). This treatment did not affect the IL-1β–induced corneal vascular loops on day 2. However, weak vascular sprouts, compared with those in controls, were observed on day 4, and a reduction in corneal neovascularization was detected on day 6. Control PBS-containing liposomes (PBS-LIPs) did not affect IL-1β–induced corneal neovascularization. Quantitative analysis demonstrated that Cl_2MDP-LIP treatment (i.v. and s.c.) significantly reduced IL-1β–induced corneal neovascularization (Figure 4, B and C) and angiogenesis on day 6. PBS-LIP treatment had no effect on VEGF-induced angiogenesis while Cl_2MDP-LIP treatment (i.v. and s.c.) inhibited VEGF-induced corneal neovascularization by approximately 50% compared with the control on day 6 (Figure 4, D and E).

IL-1β–induced angiogenesis and the infiltration of monocytes/macrophages expressing COX-2. COX-2 inhibitors block IL-1β– but not VEGF-induced angiogenesis (31). COX-$2^{-/-}$ mice lack IL-1β–induced corneal angiogenesis whereas VEGF-induced angiogenesis is not affected, suggesting that COX-2 is involved in the former (31). IL-1β–induced angiogenesis on days 4 and 6 was blocked by oral administration of a selective COX-2 inhibitor, 5,5-dimethyl-3-(3-fluorophenyl)-4-(4-methylsulphonyl)phenyl-2((5)H)-furanone (DFU) (Figure 5, A and B). On day 4, administration of DFU reduced levels of PGE_2, a main product of COX-2, in corneas by 41% of that in untreated control (Figure 5C).

$CD11b^+F4/80^+$ cells infiltrated the corneas of DFU-treated mice (Figure 5D), suggesting that COX-2 inhibition did not influence macrophage infiltration. Immunostaining with mAb F4/80 showed the infiltration of monocyte/macrophage-like cells around the neovasculature on day 4 induced by IL-1β (Figure 5E). F4/80-positive macrophages near the limbal vessel were COX-2 negative whereas those that infiltrated more deeply were COX-2 positive (Figure 5E). Thus, only activated macrophages expressed COX-2. There was no macrophage infiltration into the control corneas (data not shown).

MCP-1 in tumor growth and angiogenesis in cancer cells expressing IL-1β. We compared angiogenesis induced by Lewis lung carcinoma cells expressing IL-1β (LLC/IL-1β) and LLC cells expressing neo^R (LLC/neo) cells in a dorsal air sac assay in wild-type C57BL/6 and MCP-$1^{-/-}$ mice. Serum levels of MCP-1 and IL-1β were measured 7 days after inoculation with LLC/neo and LLC/IL-1β cells using ELISAs (Figure 6A and 6B). MCP-1 was not detected in LLC/neo-grafted or control ungrafted mice. In LLC/IL-1β–grafted wild-type mice, the serum MCP-1 concentration was 40.8 ± 5.31 pg/ml compared with 3.43 ± 0.56 pg/ml in LLC/IL-1β–grafted MCP-$1^{-/-}$ mice (Figure 6A). There were similar serum IL-1β levels in LLC/IL-1β–grafted wild-type and MCP-$1^{-/-}$ mice (334 ± 104 and 302 ± 124 pg/ml, respectively; Figure 6B). LLC/neo and LLC/IL-1β

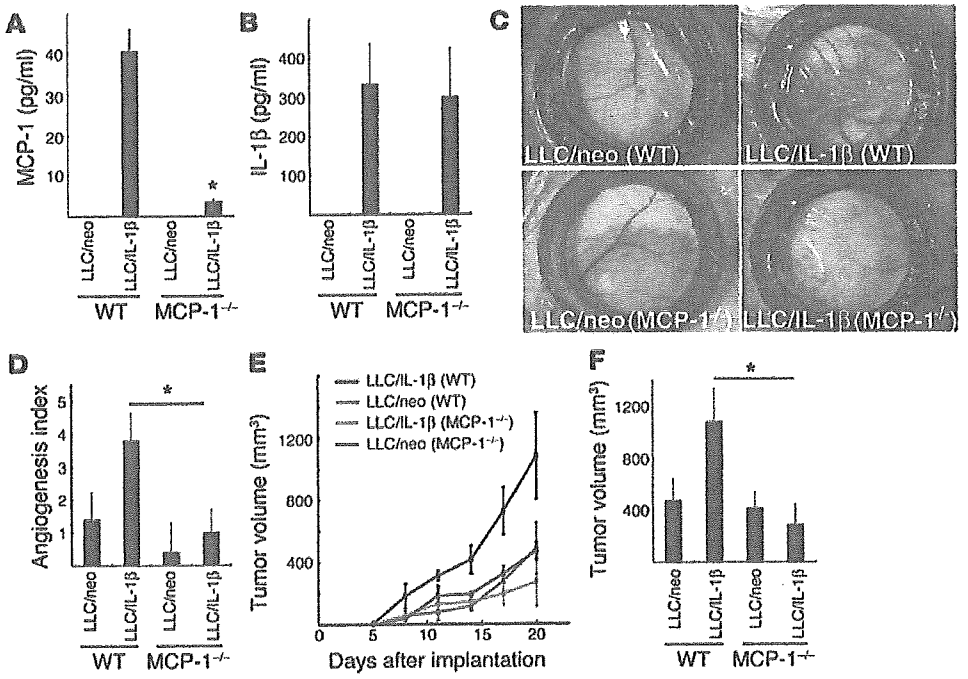

Figure 6

IL-1β–induced tumor angiogenesis in MCP-1$^{-/-}$ mice. (**A**) MCP-1 levels in the serum of LLC/IL-1β–grafted MCP-1$^{-/-}$ mice and wild-type mice 7 days after inoculation. MCP-1 was not detectable in the serum of LLC/neo-grafted mice by ELISA. Values are expressed as means ± SD of 5 samples. (**B**) IL-1β levels in the serum of LLC/IL-1β–grafted MCP-1$^{-/-}$ mice compared with wild-type mice 7 days after inoculation. *$P < 0.01$ using the unpaired Student's t test. Values are expressed as means ± SD ($n = 5$). (**C**) Representative photographs of the dorsal air sac assay with LLC/neo and LLC/IL-1β in C57BL/6 wild-type and MCP-1$^{-/-}$ mice. (**D**) Quantitative analysis of the neovascularization induced by LLC/neo or LLC/IL-1β in the dorsal air sac in wild-type and MCP-1$^{-/-}$ mice. Mean angiogenetic activities ± SD for groups of mice ($n = 5$). *$P < 0.01$ versus LLC/IL-1β using the Mann-Whitney U test. (**E**) Mean tumor volumes ± SD for groups of wild-type mice (black and red) or MCP-1$^{-/-}$ mice (green and blue) implanted with 5×10^5 LLC/IL-1β or LLC/neo cells ($n = 5$). (**F**) LLC/IL-1β tumor growth was not enhanced in MCP-1$^{-/-}$ mice ($n = 10$) compared with wild-type mice ($n = 10$; day 20). *$P < 0.01$ using the unpaired Student's t test.

cells showed identical growth rates in culture (6). IL-1β and MCP-1 are thus unlikely to promote the proliferation of LLC cells.

Implanting a chamber containing LLC/IL-1β into C57BL/6 wild-type mice produced curled microvessels and numerous tiny bleeding spots (Figure 6C). The implantation of chambers containing LLC/IL-1β into MCP-1$^{-/-}$ C57BL/6 mice produced less neovascularization than in wild-type mice. In contrast, less neovascularization was seen when LLC/neo was implanted into wild-type mice (Figure 6C). Quantitative analyses revealed 3-fold greater neovasculature development induced by LLC/IL-1β compared with LLC/neo in wild-type mice. However, implanting LLC/IL-1β into MCP-1$^{-/-}$ mice markedly reduced angiogenesis (Figure 6D).

Grafting LLC/neo or LLC/IL-1β cells into C57BL/6 wild-type and MCP-1$^{-/-}$ mice confirmed that the latter grew faster than the former in wild-type mice (Figure 6E). LLC/IL-1β–grafted tumors in MCP-1$^{-/-}$ mice were significantly smaller than in wild-type mice. There was no difference in LLC/neo tumor growth between MCP-1$^{-/-}$ and wild-type mice (Figure 6, E and F).

Selective staining of endothelial cells showed a reduction of microvascular density of approximately 50% in LLC/IL-1β tumors grafted into MCP-1$^{-/-}$ mice compared with LLC/IL-1β tumors in wild-type mice (Figure 7, A and B). Immunostaining using mAb F4/80 revealed fewer macrophages in LLC/IL-1β tumors from MCP-1$^{-/-}$ mice. However, there were similar numbers of infiltrating macrophages in LLC/neo tumors in wild-type and MCP-1$^{-/-}$ mice. Quantitative analysis revealed more F4/80-positive infiltrating macrophages in LLC/IL-1β tumors than in LLC/neo tumors (Figure 7, C and D). The number of macrophages was lower in LLC/IL-1β tumors in MCP-1$^{-/-}$ mice than in wild-type mice. It remains unclear why there were more infiltrating macrophages in LLC/neo than in LLC/IL-1β tumors, as the microvascular density was similar in both (Figure 7, B and D).

COX-2 in angiogenesis, tumor growth, and macrophage infiltration in cancer cells expressing IL-1β. Implanting a chamber containing LLC/IL-1β led to the development of microvessels (Figure 8A) while oral administration of a COX-2 inhibitor reduced this activity. Quantitative analyses revealed 3-fold greater development of the neovasculature induced by LLC/IL-1β compared with LLC/neo. Treatment with a COX-2 inhibitor significantly reduced the angiogenesis induced by LLC/IL-1β (Figure 8B).

Both LLC/IL-1β– and LLC/neo-tumor growth were inhibited by treatment with DFU, although the former was more strongly affected (Figure 8, C and D). Selective staining of endothelial cells showed the microvascular density was increased approximately 1.5-fold in LLC/IL-1β tumors compared with LLC/neo tumors grafted into mice. DFU reduced the microvascular density in LLC/IL-1β tumors but was less effective in LLC/neo tumors (Figure 8, E and F). Immunostaining revealed fewer macrophages in LLC/IL-1β tumors in DFU-treated mice compared with control mice (Figure 8G). However, there were similar numbers of infiltrating macrophages in LLC/neo tumors in control and DFU-treated mice. Quantitative analysis revealed fewer F4/80-positive infiltrating macrophages in DFU-treated LLC/IL-1β tumors compared with control tumors (Figure 8H).

Partial involvement of ELR$^+$ chemokines in IL-1β–induced angiogenesis. CXC chemokines containing the ELR motif (ELR$^+$), including IL-8, growth-related oncogenes (GRO) α, β, and γ (CXC chemokine ligand 1 [CXCL1], CXCL2, and CXCL3), and epithelial neutrophil-activating peptide-78 (ENA-78 or CXCL5), potently induce angiogenesis (35). This activity is mediated by CXC chemokine receptor 2 (CXCR2; ref. 36). Anti-CXCR2 Abs inhibited the growth of LLC/IL-1β cells in vivo (6).

We examined the levels of various ELR$^+$ CXC chemokines, including KC (CXCL1), macrophage inflammatory protein 2 (MIP-2, also known as CXCL2/3), and VEGF-A, in IL-1β–implanted corneas using ELISA. KC, MIP-2, and VEGF-A were elevated 2 days after